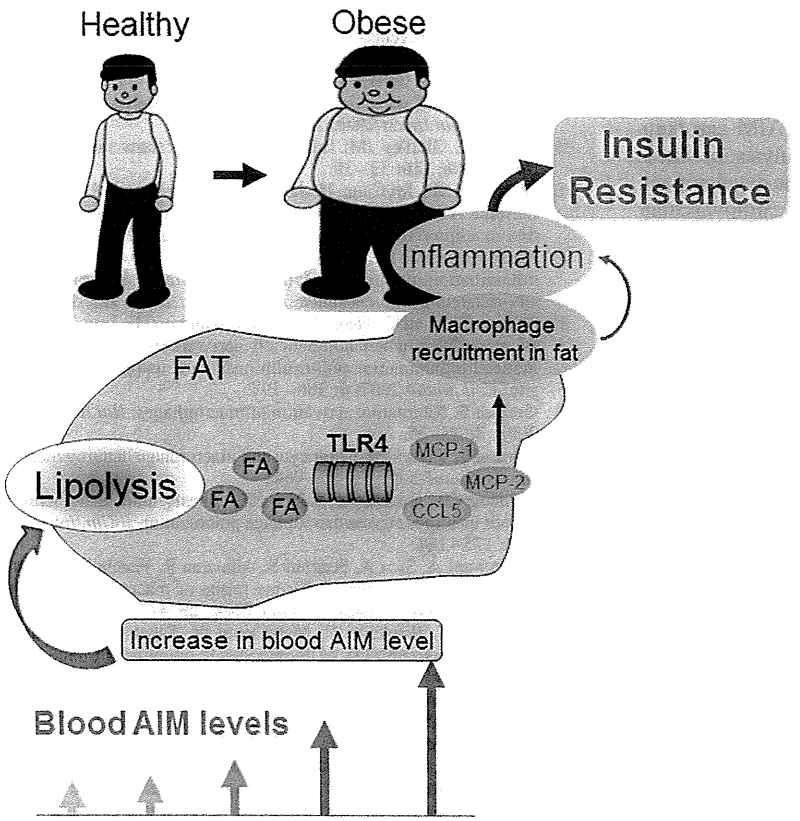

Figure 6. How apoptosis inhibitor of macrophages (AIM)-induced lipolysis contributes to macrophage recruitment in adipose tissue. FA, fatty acid.

First, suppression of *TLR4* expression by siRNA significantly reduced production of MCP-1 in 3T3-L1 adipocytes. Second, intravenous injection of rAIM into wild-type and *TLR4*$^{-/-}$ mice was assessed according to the state of lipolysis and chemokine production in epididymal adipose tissue. In wild-type and mutant mice, rAIM did induce lipolysis, as shown by increased blood FFA and glycerol levels. By contrast, induction of mRNA for chemokines by rAIM injection was significantly less efficient in *TLR4*$^{-/-}$ than in wild-type mice. Thus, in summary, AIM-induced lipolysis provoked an efflux of saturated fatty acids, including PA and SA, from adipocytes, which stimulated chemokine production in both adipocytes and resident macrophages via TLR4 activation, resulting in M1 macrophage migration (**Figure 6**). Consistent results were obtained in vivo in obese *AIM*$^{+/+}$and *AIM*$^{-/-}$ mice after 12 weeks on a HFD. In epididymal fat, phosphorylation levels of JNK, representing the state of TLR activation,[87] were decreased in *AIM*$^{-/-}$ mice compared with *AIM*$^{+/+}$ mice. In addition, chemokine mRNA levels were lower in *AIM*$^{-/-}$ compared with *AIM*$^{+/+}$ adipose tissue. Overall, these results strongly indicate that AIM-induced lipolysis is the initiating step for macrophage recruitment into obese adipose tissue.

No Inflammation or IR in Obese *AIM*$^{-/-}$ Mice

As a consequence of the abolished infiltration of inflammatory macrophages, the progression of obesity-associated inflammation is prevented both locally and systemically in obese *AIM*$^{-/-}$ mice. In adipose tissue, mRNA levels for proinflammatory cytokines such as tumor necrosis factor α (TNFα), IL-6 and IL-1β, were significantly lower in *AIM*$^{-/-}$ than in *AIM*$^{+/+}$ mice after a HFD for 12 weeks. Consistent with this finding, serum levels of TNFα and IL-6 were lower in *AIM*$^{-/-}$ mice compared with *AIM*$^{+/+}$ mice.

Activation of the insulin signaling pathway was studied after the intravenous injection of insulin in *AIM*$^{-/-}$ and *AIM*$^{+/+}$ mice fed a HFD for 12 weeks. Substantial insulin-stimulated phosphorylation of AKT and GSK3β protein kinases[88] was observed in adipose tissue, skeletal muscle (gastrocnemius), and liver in *AIM*$^{-/-}$ mice in contrast to markedly diminished phosphorylation levels in *AIM*$^{+/+}$ mice.[70] Thus, insulin sensitivity was maintained in obese *AIM*$^{-/-}$ mice. In line with this, whole-body glucose intolerance and IR observed in obese *AIM*$^{+/+}$ mice were ameliorated in obese *AIM*$^{-/-}$ mice, as shown by intraperitoneal glucose and insulin tolerance tests. Thus, *AIM*$^{-/-}$ mice showed advanced obesity compared with *AIM*$^{+/+}$ mice after a 12-week HFD, but still showed normal glucose tolerance.

Conclusion

Is AIM Beneficial or Detrimental for MetS?

AIM is incorporated into adipocytes and induces lipolysis via the reduction of FAS enzymatic activity. This decreases lipid droplet storage within adipocytes, which resists the augmentation of adipose tissue mass on overfeeding. Indeed, the weight increase of visceral fat in mice fed a HFD was accelerated in *AIM*$^{-/-}$ mice, and suppressed by the systemic administration of rAIM. Thus, AIM appears to be a beneficial molecule that impedes the progression of obesity, suggesting that it might be a promising target for next-generation anti-obesity drugs. Intriguingly, however, when this lipolytic effect is excessive

(ie, when an increased level of AIM targets hypertrophic adipocytes), it triggers chronic inflammation via the recruitment of macrophages into adipose tissue, leading to IR. In this regard, AIM is certainly detrimental for metabolic disorders. Thus, during early periods of MetS prior to prominent obesity and with limited lipid storage in adipocytes, AIM can help prevent the progression of obesity through lipolysis; in obese conditions, anti-AIM therapy should prevent the development of metabolic diseases such as diabetes and cardiovascular events, as observed in *AIM*$^{-/-}$ mice.

One of the criteria for assessing whether AIM or anti-AIM therapy should be administered is the blood AIM level, based on the observation that this increases in line with the progression of obesity in mice fed with HFD. However, 2 things are noteworthy. First, because AIM has a complicated structure, it is possible that a considerable proportion of blood AIM undergoes unsuccessful protein folding, resulting in limited or even no function. In addition, the presence of glycosylation is likely, in particular for murine AIM. Indeed, murine AIM has 3 or 4 regions susceptible to N-glycosylation, and both murine and human AIM proteins have several regions for O-glycosylation. Further, the molecular weights of both murine and human AIM are markedly larger than those estimated from their amino acid sequences, suggesting that they are heavily glycosylated. This modification may also influence the function of AIM. Therefore, not only the amount but also the activity of blood AIM should be evaluated. Second, unlike mice fed with HFD, the body mass index and AIM level are not always parallel in humans (Miyazaki, unpublished data), possibly because of the wide variation in eating habits, as some foods may induce obesity without a remarkable increase in blood AIM, and vice versa. Thus, it is relevant to study which foods increase blood AIM. It is also possible that some foods stimulate AIM production while interfering with its efficient folding and glycosylation. Thus, the evaluation of blood AIM activity together with blood AIM levels is therefore again necessary.

Practically, however, it may be difficult to clearly establish the threshold of blood AIM level or activity, which decides the agonist or antagonist to be used. To this end, large-scale cohort studies for the association of blood AIM and the incidence and levels of disease are certainly required. In the meantime, a set of parameters including blood AIM needs to be defined. In addition, development of a simple method that can maintain the AIM level at a reasonable level via modulating the expression or protein stability of AIM is required.

Perspectives

We have shown that AIM prevents the progression of obesity via lipolysis, and acts as a key factor in the initiation of obesity-associated chronic inflammation leading to IR. Future efforts to establish a diagnosis via the measurement of the blood AIM level and the therapeutic application of both AIM (AIM agonists) and anti-AIM (AIM antagonists) will further progress the development of treatments to prevent the onset of metabolic disorders brought about by the modern lifestyle.

Acknowledgments

We thank to Drs K. Nakashima and T. Kadowaki, Ms M. Mori, K. Morita, and M. Ohba for their assistance and discussion.

References

1. Hotamisligil GS, Shargill NS, Spiegelman BM. Adipose expression of tumor necrosis factor-alpha: Direct role in obesity-linked insulin resistance. *Science* 1993; **259:** 87–91.
2. Wellen KE, Hotamisligil GS. Obesity-induced inflammatory changes in adipose tissue. *J Clin Invest* 2005; **112:** 1785–1788.
3. Arkan MC, Hevener AL, Greten FR, Maeda S, Li ZW, Long JM, et al. IKK-beta links inflammation to obesity-induced insulin resistance. *Nat Med* 2005; **11:** 191–198.
4. Shoelson SE, Lee J, Goldfine AB. Inflammation and insulin resistance. *J Clin Invest* 2006; **116:** 1793–1801.
5. Neels JG, Olefsky JM. Inflamed fat: What starts the fire? *J Clin Invest* 2006; **116:** 33–35.
6. Weisberg SP, McCann D, Desai M, Rosenbaum M, Leibel RL, Ferrante AW Jr. Obesity is associated with macrophage accumulation in adipose tissue. *J Clin Invest* 2003; **112:** 1796–1808.
7. Xu H, Barnes GT, Yang Q, Tan G, Yang D, Chou CJ, et al. Chronic inflammation in fat plays a crucial role in the development of obesity-related insulin resistance. *J Clin Invest* 2003; **112:** 1821–1830.
8. Solinas G, Vilcu C, Neels JG, Bandyopadhyay GK, Luo JL, Naugler W, et al. JNK1 in hematopoietically derived cells contributes to diet-induced inflammation and insulin resistance without affecting obesity. *Cell Metab* 2007; **6:** 386–397.
9. Gordon S. Alternative activation of macrophages. *Nat Rev Immunol* 2003; **3:** 23–35.
10. Gordon S, Taylor PR. Monocyte and macrophage heterogeneity. *Nat Rev Immunol* 2005; **5:** 953–964.
11. Lumeng CN, Bodzin JL, Saltiel AR. Obesity induces a phenotypic switch in adipose tissue macrophage polarization. *J Clin Invest* 2007; **117:** 175–184.
12. Mantovani A, Sica A, Sozzani S, Allavena P, Vecchi A, Locati M. The chemokine system in diverse forms of macrophage activation and polarization. *Trends Immunol* 2004; **25:** 677–686.
13. Miyazaki T, Hirokami Y, Matsuhashi N, Takatsuka H, Naito M. Increased susceptibility of thymocytes to apoptosis in mice lacking AIM, a novel murine macrophage-derived soluble factor belonging to the scavenger receptor cysteine-rich domain superfamily. *J Exp Med* 1999; **189:** 413–422.
14. Gebe JA, Kiener PA, Ring HZ, Li X, Francke U, Aruffo A. Molecular cloning, mapping to human chromosome 1 q21–q23, and cell binding characteristics of Spalpha, a new member of the scavenger receptor cysteine-rich (SRCR) family of proteins. *J Biol Chem* 1997; **272:** 6151–6158.
15. Gebe JA, Llewellyn M, Hoggatt H, Aruffo A. Molecular cloning, genomic organization and cell-binding characteristics of mouse Spalpha. *Immunology* 2000; **99:** 78–86.
16. Gangadharan B, Antrobus R, Dwek RA, Zitzmann N. Novel serum biomarker candidates for liver fibrosis in hepatitis C patients. *Clin Chem* 2007; **53:** 1792–1799.
17. Kim WK, Hwang HR, Kim do H, Lee PY, In YJ, Ryu HY, et al. Glycoproteomic analysis of plasma from patients with atopic dermatitis: CD5L and ApoE as potential biomarkers. *Exp Mol Med* 2009; **40:** 677–685.
18. Gray J, Chattopadhyay D, Beale GS, Patman GL, Miele L, King BP, et al. A proteomic strategy to identify novel serum biomarkers for liver cirrhosis and hepatocellular cancer in individuals with fatty liver disease. *BMC Cancer* 2009; **9:** 271.
19. Joseph SB, Bradley MN, Castrillo A, Bruhn KW, Mak PA, Pei L, et al. LXR-dependent gene expression is important for macrophage survival and the innate immune response. *Cell* 2004; **119:** 299–309.
20. Valledor AF, Hsu LC, Ogawa S, Sawka-Verhelle D, Karin M, Glass CK. Activation of liver X receptors and retinoid X receptors prevents bacterial-induced macrophage apoptosis. *Proc Natl Acad Sci USA* 2004; **101:** 17813–17818.
21. Shibata N, Glass CK. Macrophages, oxysterols and atherosclerosis. *Circ J* 2010; **74:** 2045–2051.
22. Arai S, Shelton JM, Chen M, Bradley MN, Castrillo A, Bookout AL, et al. A role of the apoptosis inhibitory factor AIM/Spalpha/Api6 in atherosclerosis development. *Cell Metab* 2005; **1:** 201–213.
23. Yusa S, Ohnishi S, Onodera T, Miyazaki T. AIM, a murine apoptosis inhibitory factor, induces strong and sustained growth inhibition of B lymphocytes in combination with TGF-beta1. *Eur J Immunol* 1999; **29:** 1086–1093.
24. Kuwata K, Watanabe H, Jiang SY, Yamamoto T, Tomiyama-Miyaji C, Abo T, et al. AIM inhibits apoptosis of T cells and NKT cells in *Corynebacterium*-induced granuloma formation in mice. *Am J Pathol* 2003; **162:** 837–847.
25. Qu P, Du H, Li Y, Yan C. Myeloid-specific expression of Api6/AIM/Sp alpha induces systemic inflammation and adenocarcinoma in the lung. *J Immunol* 2009; **182:** 1648–1659.
26. Kurokawa J, Arai S, Nakashima K, Nishijima A, Miyake K, Ose R, et al. AIM is endocytosed into adipocytes and decreases lipid droplets via inhibition of fatty acid synthase activity. *Cell Metab* 2010; **11:** 479–492.

27. Zechner R, Strauss JG, Haemmerle G, Lass A, Zimmermann R. Lipolysis: Pathway under construction. *Curr Opin Lipidol* 2005; **16:** 333–340.
28. Duncan RE, Ahmadian M, Jaworski K, Sarkadi-Nagy E, Sul HS. Regulation of lipolysis in adipocytes. *Annu Rev Nutr* 2007; **27:** 79–101.
29. Madsen L, Petersen RK, Sorensen MB, Jorgensen C, Hallenborg P, Pridal L, et al. Adipocyte differentiation of 3T3-L1 preadipocytes is dependent on lipoxygenase activity during the initial stages of the differentiation process. *Biochem J* 2003; **375:** 539–549.
30. Olsnes S, Klingenberg O, Wiedłocha A. Transport of exogenous growth factors and cytokines to the cytosol and to the nucleus. *Physiol Rev* 2003; **83:** 163–182.
31. Wesche J, Małecki J, Wiedłocha A, Skjerpen CS, Claus P, Olsnes S. FGF-1 and FGF-2 require the cytosolic chaperone Hsp90 for translocation into the cytosol and the cell nucleus. *J Biol Chem* 2006; **281:** 11405–11412.
32. Lin SY, Makino K, Xia W, Matin A, Wen Y, Kwong KY, et al. Nuclear localization of EGF receptor and its potential new role as a transcription factor. *Nat Cell Biol* 2001; **3:** 802–808.
33. Sandvig K, van Deurs B. Entry of ricin and Shiga toxin into cells: Molecular mechanisms and medical perspectives. *EMBO J* 2000; **19:** 5943–5950.
34. Sandvig K, van Deurs B. Delivery into cells: Lessons learned from plant and bacterial toxins. *Gene Ther* 2005; **12:** 865–872.
35. Ackerman AL, Kyritsis C, Tampé R, Cresswell P. Access of soluble antigens to the endoplasmic reticulum can explain cross-presentation by dendritic cells. *Nat Immunol* 2005; **6:** 107–113.
36. Giodini A, Cresswell P. Hsp90-mediated cytosolic refolding of exogenous proteins internalized by dendritic cells. *EMBO J* 2008; **27:** 201–211.
37. Greenwalt DE, Lipsky RH, Ockenhouse CF, Ikeda H, Tandon NN, Jamieson GA. Membrane glycoprotein CD36: A review of its roles in adherence, signal transduction, and transfusion medicine. *Blood* 1992; **80:** 1105–1115.
38. Ibrahimi A, Abumrad NA. Role of CD36 in membrane transport of long-chain fatty acids. *Curr Opin Clin Nutr Metab Care* 2002; **5:** 139–145.
39. Febbraio M, Abumrad NA, Hajjar DP, Sharma K, Cheng W, Pearce SF, et al. A null mutation in murine CD36 reveals an important role in fatty acid and lipoprotein metabolism. *J Biol Chem* 1999; **274:** 19055–19062.
40. Silverstein RL, Li W, Park YM, Rahaman SO. Mechanisms of cell signaling by the scavenger receptor CD36: Implications in atherosclerosis and thrombosis. *Trans Am Clin Climatol Assoc* 2010; **121:** 206–220.
41. Nicholson AC, Febbraio M, Han J, Silverstein RL, Hajjar DP. CD36 in atherosclerosis: The role of a class B macrophage scavenger receptor. *Ann NY Acad Sci* 2000; **902:** 128–133.
42. Chirala SS, Chang H, Matzuk M, Abu-Elheiga L, Mao J, Mahon K, et al. Fatty acid synthesis is essential in embryonic development: Fatty acid synthase null mutants and most of the heterozygotes die in utero. *Proc Natl Acad Sci USA* 2003; **100:** 6358–6363.
43. Smith S, Stern A, Randhawa ZI, Knudsen J. Mammalian fatty acid synthetase is a structurally and functionally symmetrical dimer. *Eur J Biochem* 1985; **52:** 547–555.
44. Asturias FJ, Chadick JZ, Cheung IK, Stark H, Witkowski A, Joshi AK, et al. Structure and molecular organization of mammalian fatty acid synthase. *Nat Struct Mol Biol* 2005; **12:** 225–232.
45. Kuhajda FP, Pizer ES, Li JN, Mani NS, Frehywot GL, Townsend CA. Synthesis and antitumor activity of an inhibitor of fatty acid synthase. *Proc Natl Acad Sci USA* 2000; **97:** 3450–3454.
46. Schmid B, Rippmann JF, Tadayyon M, Hamilton BS. Inhibition of fatty acid synthase prevents preadipocyte differentiation. *Biochem Biophys Res Commun* 2005; **328:** 1073–1082.
47. Rosen ED, Sarraf P, Troy AE, Bradwin G, Moore K, Milstone DS, et al. PPAR gamma is required for the differentiation of adipose tissue in vivo and in vitro. *Mol Cell* 1999; **4:** 611–617.
48. Farmer SR. Transcriptional control of adipocyte formation. *Cell Metab* 2006; **4:** 263–273.
49. Wu Z, Puigserver P, Spiegelman BM. Transcriptional activation of adipogenesis. *Curr Opin Cell Biol* 1999; **11:** 689–694.
50. Loftus TM, Jaworsky DE, Frehywot GL, Townsend CA, Ronnett GV, Lane MD, et al. Reduced food intake and body weight in mice treated with fatty acid synthase inhibitors. *Science* 2000; **288:** 2379–2381.
51. Makimura H, Mizuno TM, Yang XJ, Silverstein J, Beasley J, Mobbs CV. Cerulenin mimics effects of leptin on metabolic rate, food intake, and body weight independent of the melanocortin system, but unlike leptin, cerulenin fails to block neuroendocrine effects of fasting. *Diabetes* 2001; **50:** 733–739.
52. Kumar MV, Shimokawa T, Nagy TR, Lane MD. Differential effects of a centrally acting fatty acid synthase inhibitor in lean and obese mice. *Proc Natl Acad Sci USA* 2002; **99:** 1921–1925.
53. Mobbs CV, Makimura H. Block the FAS, lose the fat. *Nat Med* 2002; **8:** 335–336.
54. Shimokawa T, Kumar MV, Lane MD. Effect of a fatty acid synthase inhibitor on food intake and expression of hypothalamic neuropeptides. *Proc Natl Acad Sci USA* 2002; **99:** 66–71.
55. Kovacs P, Harper I, Hanson RL, Infante AM, Bogardus C, Tataranni PA, et al. A novel missense substitution (Val1483Ile) in the fatty acid synthase gene (FAS) is associated with percentage of body fat and substrate oxidation rates in nondiabetic Pima Indians. *Diabetes* 2004; **53:** 1915–1919.
56. Liu LH, Wang XK, Hu YD, Kang JL, Wang LL, Li S. Effects of a fatty acid synthase inhibitor on adipocyte differentiation of mouse 3T3-L1 cells. *Acta Pharmacol Sin* 2004; **25:** 1052–1057.
57. Ronnett GV, Kim EK, Landree LE, Tu Y. Fatty acid metabolism as a target for obesity treatment. *Physiol Behav* 2005; **85:** 25–35.
58. Chakravarthy MV, Zhu Y, Yin L, Coleman T, Pappan KL, Marshall CA, et al. Inactivation of hypothalamic FAS protects mice from diet-induced obesity and inflammation. *J Lipid Res* 2009; **50:** 630–640.
59. Wu Z, Rosen ED, Brun R, Hauser S, Adelmant G, Troy AE, et al. Cross-regulation of C/EBP alpha and PPAR gamma controls the transcriptional pathway of adipogenesis and insulin sensitivity. *Mol Cell* 1999; **3:** 151–158.
60. He W, Barak Y, Hevener A, Olson P, Liao D, Le J, et al. Adipose-specific peroxisome proliferator-activated receptor gamma knockout causes insulin resistance in fat and liver but not in muscle. *Proc Natl Acad Sci USA* 2003; **100:** 15712–15717.
61. Holm C. Molecular mechanisms regulating hormone-sensitive lipase and lipolysis. *Biochem Soc Trans* 2003; **31:** 1120–1124.
62. Finn PF, Dice JF. Proteolytic and lipolytic responses to starvation. *Nutrition* 2006; **22:** 830–844.
63. Zechner R, Kienesberger PC, Haemmerle G, Zimmermann R, Lass A. Adipose triglyceride lipase and the lipolytic catabolism of cellular fat stores. *J Lipid Res* 2009; **50:** 3–21.
64. Girousse A, Langin D. Adipocyte lipases and lipid droplet-associated proteins: Insight from transgenic mouse models. *Int J Obes (Lond)* 2011 June 14 [E-pub ahead of print].
65. Lafontan M. Advances in adipose tissue metabolism. *Int J Obes* 2008; **32**(Suppl 7): S39–S51.
66. Ozcan U, Cao Q, Yilmaz E, Lee AH, Iwakoshi NN, Ozdelen E, et al. Endoplasmic reticulum stress links obesity, insulin action, and type 2 diabetes. *Science* 2006; **306:** 457–461.
67. Kahn SE, Hull RL, Utzschneider KM. Mechanisms linking obesity to insulin resistance and type 2 diabetes. *Nature* 2006; **444:** 840–846.
68. Sutherland LN, Capozzi LC, Turchinsky NJ, Bell RC, Wright DC. Time course of high-fat diet-induced reductions in adipose tissue mitochondrial proteins: Potential mechanisms and the relationship to glucose intolerance. *Am J Physiol Endocrinol Metab* 2008; **295:** E1076–E1083.
69. Kosteli A, Sugaru E, Haemmerle G, Martin JF, Lei J, Zechner R, et al. Weight loss and lipolysis promote a dynamic immune response in murine adipose tissue. *J Clin Invest* 2010; **120:** 3466–3479.
70. Kurokawa J, Nagano H, Ohara O, Kubota N, Kadowaki T, Arai S, et al. Apoptosis inhibitor of macrophage (AIM) is required for obesity-associated recruitment of inflammatory macrophages into adipose tissue. *Proc Natl Acad Sci USA* 2011; **108:** 12072–12077.
71. Wu H, Ghosh S, Perrard XD, Feng L, Garcia GE, Perrard JL, et al. T-cell accumulation and regulated on activation, normal T cell expressed and secreted upregulation in adipose tissue in obesity. *Circulation* 2007; **115:** 1029–1038.
72. Kintscher U, Hartge M, Hess K, Foryst-Ludwig A, Clemenz M, Wabitsch M, et al. T-lymphocyte infiltration in visceral adipose tissue: A primary event in adipose tissue inflammation and the development of obesity-mediated insulin resistance. *Arterioscler Thromb Vasc Biol* 2008; **28:** 1304–1310.
73. Feuerer M, Herrero L, Cipolletta D, Naaz A, Wong J, Nayer A, et al. Lean, but not obese, fat is enriched for a unique population of regulatory T cells that affect metabolic parameters. *Nat Med* 2009; **15:** 930–939.
74. Nishimura S, Manabe I, Nagasaki M, Eto K, Yamashita H, Ohsugi M, et al. CD8+ effector T cells contribute to macrophage recruitment and adipose tissue inflammation in obesity. *Nat Med* 2009; **15:** 914–920.
75. Winer S, Chan Y, Paltser G, Truong D, Tsui H, Bahrami J, et al. Normalization of obesity-associated insulin resistance through immunotherapy. *Nat Med* 2009; **15:** 921–929.

76. Shi H, Kokoeva MV, Inouye K, Tzameli I, Yin H, Flier JS. TLR4 links innate immunity and fatty acid-induced insulin resistance. *J Clin Invest* 2006; **116:** 3015–3025.
77. Suganami T, Tanimoto-Koyama K, Nishida J, Itoh M, Yuan X, Mizuarai S, et al. Role of the Toll-like receptor 4/NF-κB pathway in saturated fatty acid-induced inflammatory changes in the interaction between adipocytes and macrophages. *Arterioscler Thromb Vasc Biol* 2007; **27:** 84–91.
78. Poggi M, Bastelica D, Gual P, Iglesias MA, Gremeaux T, Knauf C, et al. C3H/HeJ mice carrying a toll-like receptor 4 mutation are protected against the development of insulin resistance in white adipose tissue in response to a high-fat diet. *Diabetologia* 2007; **50:** 1267–1276.
79. Tsukumo DM, Carvalho-Filho MA, Carvalheira JB, Prada PO, Hirabara SM, Schenka AA, et al. Loss-of-function mutation in Toll-like receptor 4 prevents diet-induced obesity and insulin resistance. *Diabetes* 2007; **56:** 1986–1998.
80. Davis JE, Gabler NK, Walker-Daniels J, Spurlock ME. Tlr-4 deficiency selectively protects against obesity induced by diets high in saturated fat. *Obesity* 2008; **16:** 1248–1255.
81. Kamei N, Tobe K, Suzuki R, Ohsugi M, Watanabe T, Kubota N, et al. Overexpression of monocyte chemoattractant protein-1 in adipose tissues causes macrophage recruitment and insulin resistance. *J Biol Chem* 2006; **281:** 26602–26614.
82. Kanda H, Tateya S, Tamori Y, Kotani K, Hiasa K, Kitazawa R, et al. MCP-1 contributes to macrophage infiltration into adipose tissue, insulin resistance, and hepatic steatosis in obesity. *J Clin Invest* 2006; **116:** 1494–1505.
83. Keophiphath M, Rouault C, Divoux A, Clément K, Lacasa D. CCL5 promotes macrophage recruitment and survival in human adipose tissue. *Arterioscler Thromb Vasc Biol* 2010; **30:** 39–45.
84. Soma MR, Mims MP, Chari MV, Rees D, Morrisett JD. Triglyceride metabolism in 3T3-L1 cells: An in vivo ^{13}C NMR study. *J Biol Chem* 1992; **267:** 11168–11175.
85. Kopp A, Gross P, Falk W, Bala M, Weigert J, Buechler C, et al. Fatty acids as metabolic mediators in innate immunity. *Eur J Clin Invest* 2009; **39:** 924–933.
86. Schaeffler A, Gross P, Buettner R, Bollheimer C, Buechler C, Neumeier M, et al. Fatty acid-induced induction of Toll-like receptor-4/nuclear factor-kappaB pathway in adipocytes links nutritional signalling with innate immunity. *Immunology* 2009; **126:** 233–245.
87. Jenkins KA, Mansell A. TIR-containing adaptors in Toll-like receptor signalling. *Cytokine* 2010; **49:** 237–244.
88. Miura T, Miki T. GSK-3beta, a therapeutic target for cardiomyocyte protection. *Circ J* 2009; **73:** 1184–1192.

Apoptosis inhibitor of macrophage (AIM) is required for obesity-associated recruitment of inflammatory macrophages into adipose tissue

Jun Kurokawa[a], Hiromichi Nagano[a], Osamu Ohara[b], Naoto Kubota[c], Takashi Kadowaki[c], Satoko Arai[a], and Toru Miyazaki[a,1]

[a]Laboratory of Molecular Biomedicine for Pathogenesis, Center for Disease Biology and Integrative Medicine, Faculty of Medicine, University of Tokyo, Tokyo 113-0033, Japan; [b]Department of Human Genome Research, Kazusa DNA Research Institute, Kisarazu, Chiba 292-0818, Japan; and [c]Department of Internal Medicine, Graduate School of Medicine, University of Tokyo, Tokyo 113-0033, Japan

Edited* by Tadatsugu Taniguchi, University of Tokyo, Tokyo, Japan, and approved June 14, 2011 (received for review February 3, 2011)

Infiltration of inflammatory macrophages into adipose tissues with the progression of obesity triggers insulin resistance and obesity-related metabolic diseases. We recently reported that macrophage-derived apoptosis inhibitor of macrophage (AIM) protein is increased in blood in line with obesity progression and is incorporated into adipocytes, thereby inducing lipolysis in adipose tissue. Here we show that such a response is required for the recruitment of adipose tissue macrophages. In vitro, AIM-dependent lipolysis induced an efflux of palmitic and stearic acids from 3T3-L1 adipocytes, thereby stimulating chemokine production in adipocytes via activation of toll-like receptor 4 (TLR4). In vivo administration of recombinant AIM to *TLR4*-deficient (*TLR4*$^{-/-}$) mice resulted in induction of lipolysis without chemokine production in adipose tissues. Consistently, mRNA levels for the chemokines that affect macrophages were far lower in *AIM*-deficient (*AIM*$^{-/-}$) than in wild-type (*AIM*$^{+/+}$) obese adipose tissue. This reduction in chemokine production resulted in a marked prevention of inflammatory macrophage infiltration into adipose tissue in obese *AIM*$^{-/-}$ mice, although these mice showed more advanced obesity than *AIM*$^{+/+}$ mice on a high-fat diet. Diminished macrophage infiltration resulted in decreased inflammation locally and systemically in obese *AIM*$^{-/-}$ mice, thereby protecting them from insulin resistance and glucose intolerance. These results indicate that the increase in blood AIM is a critical event for the initiation of macrophage recruitment into adipose tissue, which is followed by insulin resistance. Thus, AIM suppression might be therapeutically applicable for the prevention of obesity-related metabolic disorders.

diabetes | fatty acid synthase | CD36 | knockout mouse

Chronic, low-grade inflammation observed in adipose tissues is characteristic of obesity. Such a subclinical inflammatory state of adipose tissues is highly associated with insulin resistance both in adipose tissue and systemically and thus contributes to the development of multiple obesity-induced metabolic and cardiovascular diseases (1–4). Evidence has shown that infiltration of a large number of classically activated inflammatory macrophages (M1 macrophages) into adipose tissue is responsible for obesity-associated inflammation (5–7). Lean adipose tissue contains a resident population of alternatively activated macrophages (M2 macrophages), which can suppress the inflammation of both adipocytes and macrophages partly via the secretion of interleukin (IL)-10. Hence, obesity induces a switch in macrophage activation state in adipose tissue toward M1 polarization, which leads to inflammation (8–12). However, the mechanism that promotes infiltration of inflammatory macrophages into obese adipose tissue is as yet unknown.

We recently reported that the apoptosis inhibitor of macrophage (AIM) protein (13) is incorporated into adipocytes via CD36-mediated endocytosis, and induces lipolysis by suppressing the activity of fatty acid synthase (FAS) (14). AIM is a member of the scavenger receptor cysteine-rich superfamily and was initially identified as an apoptosis inhibitor that supports the survival of macrophages against different types of apoptosis-inducing stimuli (13). AIM is a direct target for regulation by nuclear receptor liver X receptor/retinoid X receptor (LXR/RXR) heterodimers (15, 16) and is solely produced by tissue macrophages. As a secreted molecule, AIM is detected in both human and mouse blood at various levels (13, 16–19) and increases in blood with the progression of obesity in mice fed a high-fat diet (HFD) (14). The augmented blood AIM induced lipolysis, as evident by the fact that the increase of free fatty acids (FFAs) and glycerol in blood was suppressed in *AIM*$^{-/-}$ mice (14). Owing to less lipolysis, adipocyte hypertrophy was more advanced and the overall mass of visceral adipose tissues was greater in *AIM*$^{-/-}$ than in *AIM*$^{+/+}$ mice fed a HFD (14). All these observations imply that AIM-induced lipolysis might be responsible for the obesity-associated recruitment of adipose tissue macrophages.

In the present study, we assessed whether AIM affects macrophage accumulation in adipose tissues in obese mice. In addition, we determined the molecular mechanism of how AIM-dependent lipolysis results in the production of chemokines by adipocytes for the effective recruitment of adipose tissue macrophages. Finally, we investigated how the absence of AIM influences the local and systemic inflammatory state and insulin resistance in mice. On the basis of these results, we discuss the putative role of AIM in the initiation of obesity-associated chronic inflammation and subsequent metabolic diseases.

Results and Discussion

Prevention of M1 Macrophage Recruitment into Adipose Tissues in Obese *AIM*$^{-/-}$ Mice. In *AIM*$^{-/-}$ mice, adipocyte hypertrophy was more advanced than in *AIM*$^{+/+}$ mice, and the overall mass of visceral fat as well as body weight was markedly greater compared with that of *AIM*$^{+/+}$ mice (14). Interestingly, however, far fewer macrophages stained with a pan-macrophage antibody F4/80 were observed in epididymal adipose tissue in *AIM*$^{-/-}$ mice than in *AIM*$^{+/+}$ mice fed a HFD for 12 wk (Fig. 1*A*). The number of IL-6 stained inflammatory type (M1) macrophages in obese *AIM*$^{-/-}$ mice was markedly lower than in obese *AIM*$^{+/+}$ mice (Fig. 1*A*). In addition, almost no M1 macrophage clusters forming crown-like structures (CLS) were observed in obese *AIM*$^{-/-}$ mice (Fig. 1*A*). In contrast, the number of M2 adipose tissue macrophages stained for mannose receptor (MR) was not increased in *AIM*$^{+/+}$ or *AIM*$^{-/-}$ mice after a 12-wk HFD (Fig. 1*B*). Furthermore, the stromal-vascular cell fraction (SVF) containing macrophages was isolated from the epididymal fat tissue of lean and obese mice by collagenase treatment and

Author contributions: T.M. designed research; J.K., O.O., N.K., and S.A. performed research; H.N. contributed new reagents/analytic tools; J.K., O.O., T.K., and T.M. analyzed data; and S.A. and T.M. wrote the paper.

The authors declare no conflict of interest.

*This Direct Submission article had a prearranged editor.

[1]To whom correspondence should be addressed. E-mail: tm@m.u-tokyo.ac.jp.

This article contains supporting information online at www.pnas.org/lookup/suppl/doi:10.1073/pnas.1101841108/-/DCSupplemental.

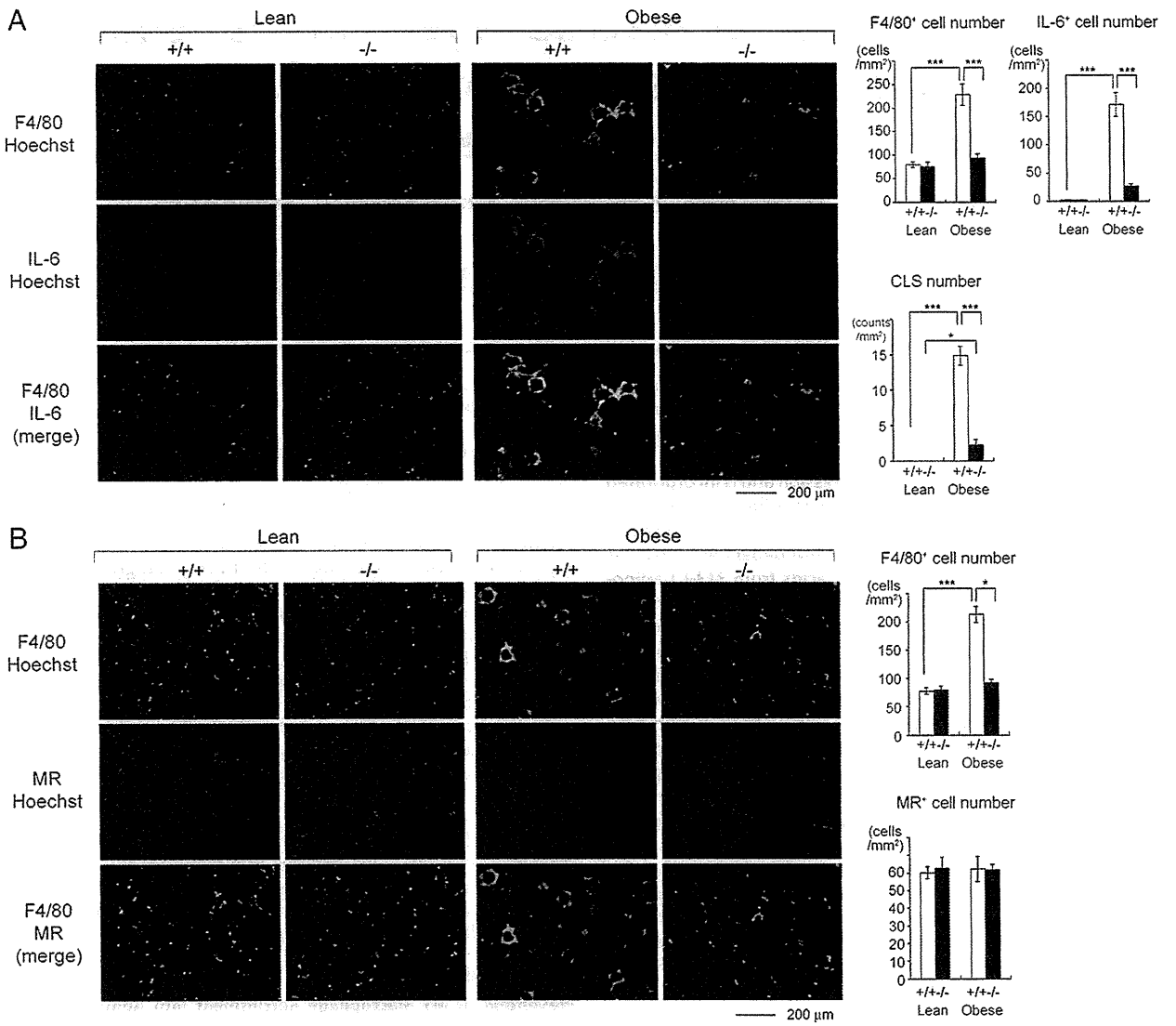

Fig. 1. Requirement of AIM for macrophage recruitment into obese adipose tissue. (*A* and *B*) Specimens of epididymal fat tissue from lean (0 wk) or obese (fed a HFD for 12 wk) $AIM^{+/+}$ and $AIM^{-/-}$ mice were costained for F4/80 (pan-macrophage marker; green), IL-6 (red), and Hoechst (blue) for *A*, and F4/80 (pan-macrophage marker; green), mannose receptor (MR) (red), and Hoechst (blue) for *B*. (Scale bar, 200 μm.) Quantification of F4/80⁺ cell number, IL-6⁺ macrophages, and the number of crown-like structures (CLS) are presented for *A*, or F4/80⁺ cell number and MR⁺ macrophages for *B* are presented. At least three different areas in three different sections per mouse were analyzed in six to eight mice of each genotype. Results are presented as averages ± SEM.

assessed to determine the number of both types of macrophage by flow cytometry after staining for F4/80 and CD11b (macrophage), CD11c (M1 marker), and MR. Consistent with the histological data, the increase in M1 macrophage number was apparent in obese $AIM^{+/+}$ but not in obese $AIM^{-/-}$ mice (Fig. S1*A*). The M1/M2 ratio of macrophage number was significantly increased in obese $AIM^{+/+}$ than in lean $AIM^{+/+}$ mice, indicating M1 polarization of adipose tissue macrophage (9), whereas this was comparable in lean and obese $AIM^{-/-}$ mice (Fig. S1*B*). Similarly, quantitative RT-PCR (QPCR) analysis with RNA isolated from epididymal fat showed a remarkable increase in mRNA levels for M1 macrophage marker genes, such as *CD11c* and *iNOS*, after a 12-wk HFD in $AIM^{+/+}$ mice, whereas this was not apparent in $AIM^{-/-}$ mice (Fig. S1*C*). In addition, expression levels of antiinflammatory (M2) macrophage marker genes, such as *CD163*, *MR*, and *arginase*, were decreased in epididymal fat of $AIM^{+/+}$ mice fed a HFD, whereas this was not observed in $AIM^{-/-}$ mice (Fig. S1*C*). The reduction in mRNA levels of M2 markers in obese $AIM^{+/+}$ mice is consistent with the increase in the M1/M2 ratio of macrophage number in obese $AIM^{+/+}$ mice (Fig. 1*D*). The difference in macrophage accumulation in fat in the presence or absence of AIM was not predominantly brought about by the antiapoptotic effect of AIM (13, 20) because the apoptotic state of macrophages (and also of adipocytes) was comparable between obese $AIM^{+/+}$ and $AIM^{-/-}$ epididymal adipose tissues, as assessed by TUNEL staining (Fig. S2). These results implicate an indispensable role of AIM in the obesity-associated recruitment of adipose tissue macrophages.

AIM-Dependent Lipolysis Induces Macrophage Migration. We then tested whether AIM itself attracts macrophages. However, AIM showed no chemoattractive activity in a macrophage migration assay using RAW264.1 mouse macrophage cells (Fig. 2*A*, *Left*). In contrast, conditioned medium from 3T3-L1 adipocytes that had been challenged with rAIM for 72 h (AIM CM) efficiently attracted macrophage cells (Fig. 2*A*, *Left*). A comparable effect was observed with conditioned medium from cells treated with C75, a specific FAS inhibitor that also induces lipolysis (14). AIM CM also attracted

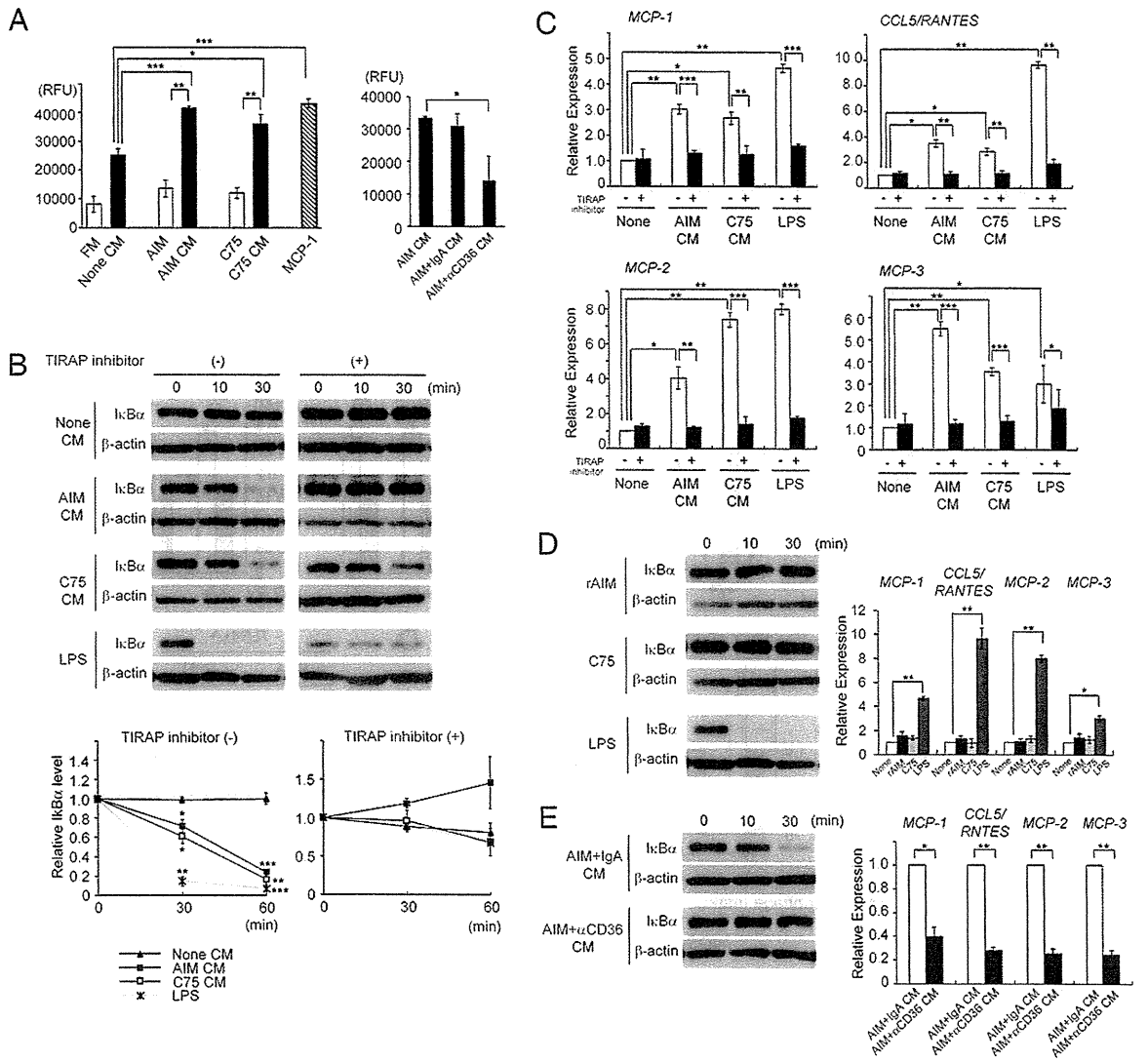

Fig. 2. AIM-dependent lipolysis induces chemokine production in adipocytes via TLR4 stimulation. (*A*) Chemotaxis of RAW 264.1 cells in response to specified stimulant. Attractants: rAIM (25 μg/mL), C75 (25 μM), AIM CM/C75 CM: conditioned medium from 3T3-L1 adipocytes treated for 3 d with rAIM (25 μg/mL) or C75 (25 μM), respectively; AIM+αCD36 CM/AIM+IgA CM: conditioned medium from 3T3-L1 adipocytes treated for 3 d with rAIM (25 μg/mL) in the presence of anti-CD36 Ab or mouse IgA (10 μg/mL each), respectively; none CM, control CM: treated without rAIM or C75; and FM: fresh DMEM culture medium containing 10% FBS. Averages from $n = 3 \pm$ SEM. MCP-1 (100 ng/mL) was used as a positive control. (*B*) Degradation of IkBα in 3T3-L1 adipoctytes in response to specified stimulant in the absence (−) or presence (+) of a TIRAP inhibitor (100 μM). LPS (100 ng/mL) was used as a positive control. Representative immunoblotting results are presented. The density of the signal was quantified using National Institutes of Health Image J image analysis software and presented as values relative to those of prestimulation (*Lower* two panels). $n = 3$. Error bar: SEM. *, versus the value at prestimulation (0 min). (*C*) QPCR analysis of mRNA levels for *MCP-1*, *CCL5/RANTES*, *MCP-2*, and *MCP-3* using RNA isolated from 3T3-L1 adipocytes treated with specified stimulant for 24 h in the absence (white bars) or presence (black bars) of a TIRAP inhibitor. Values were presented as relative expression to those without stimulation (none). $n = 3$ for each. Error bar: SEM. (*D* and *E*) No degradation of IkBα or expression induction of mRNA for chemokine genes in 3T3-L1 adipoctytes in response to rAIM alone (25 μg/mL) (*D*) or AIM+αCD36 CM (*E*).

J774.1 mouse monocyte cells (Fig. S3*A*). Furthermore, 3T3-L1 adipocytes were treated with rAIM in the presence of a CD36-neutralizing antibody (mouse IgA), which inhibits AIM-dependent lipolysis by disturbing the endocytosis of AIM into adipocytes (14), and the conditioned medium (AIM+αCD36 CM) was assessed in the macrophage migration assay. The AIM+αCD36 CM did not efficiently attract macrophages (Fig. 2*A*, *Right*), suggesting that AIM-induced lipolysis in adipocytes appears to be responsible for macrophage recruitment. The CD36-neutralizing antibody itself had no direct effect on the macrophage migration (Fig. S3*B*).

Fatty Acids Effluxed from Adipocytes in Response to AIM-Dependent Lipolysis Stimulated TLR Signaling Pathway and Induced Chemokine Production in Adipocytes. Accumulating evidence has demonstrated that saturated fatty acids activate TLR signaling cascade and that this response is tightly associated with obesity-induced inflammation (21–25). Thus, it is plausible that an increase in blood AIM may induce vigorous lipolysis in obese adipose tissues, and saturated fatty acids effluxed from adipocytes as a result of lipolysis might activate chemokine production in adipocytes via the stimulation of TLR(s) in a paracrine/autocrine fashion (26–28). Indeed, palmitic and stearic acids, the major fatty acids comprising triglyceride droplets (29) and well known as stimulators of TLR4 and TLR2 (21, 25, 30, 31), were identified as the components released by adipocytes in response to lipolysis induced by AIM or C75 when the profile of fatty acids in AIM CM and C75 CM was evaluated by gas-chromatography mass-spectrometry analysis.

Consistent with this result, both AIM CM and C75 CM efficiently stimulated the TLR signaling cascade and chemokine production in 3T3-L1 adipocytes, as assessed by degradation of IkBα (Fig. 2*B*) and mRNA expression of chemokines such as *MCP-1*, *CCL5/RANTES*, *MCP-2*, and *MCP-3*, which affects macrophages (Fig. 2*C*). AIM CM induced substantial levels of protein of these chemokines as assessed by ELISA (Fig. S4*A*). These responses diminished when adipocytes were treated with AIM CM or C75 CM in the presence of a toll–interleukin-1 receptor domain containing adapter protein (TIRAP) inhibitor, which specifically interferes with the interaction of TLR4 (as well as TLR2) and the adapter protein TIRAP/Mal, resulting in attenuation of TLR signaling (Fig. 2 *B* and *C*) (32). Furthermore, we confirmed that similar effects of TLR activation and chemokine production were observed when 3T3-L1 adipocytes were treated with palmitic acid (PA) or stearic acid (SA) and that the responses induced by each fatty acid were reduced when subjected to the TIRAP inhibitor (Fig. S5). Consistent with the results from macrophage migration assay presented in Fig. 2*A*, neither rAIM alone (Fig. 2*D* and Fig. S4*B*) nor AIM+αCD36 CM (Fig. 2*E* and Fig. S4*C*) stimulated IkBα degradation or chemokine mRNA and protein expression in adipocytes. These findings clearly indicate the necessity of the lipolytic process in the overall activation of TLR signaling cascade by AIM.

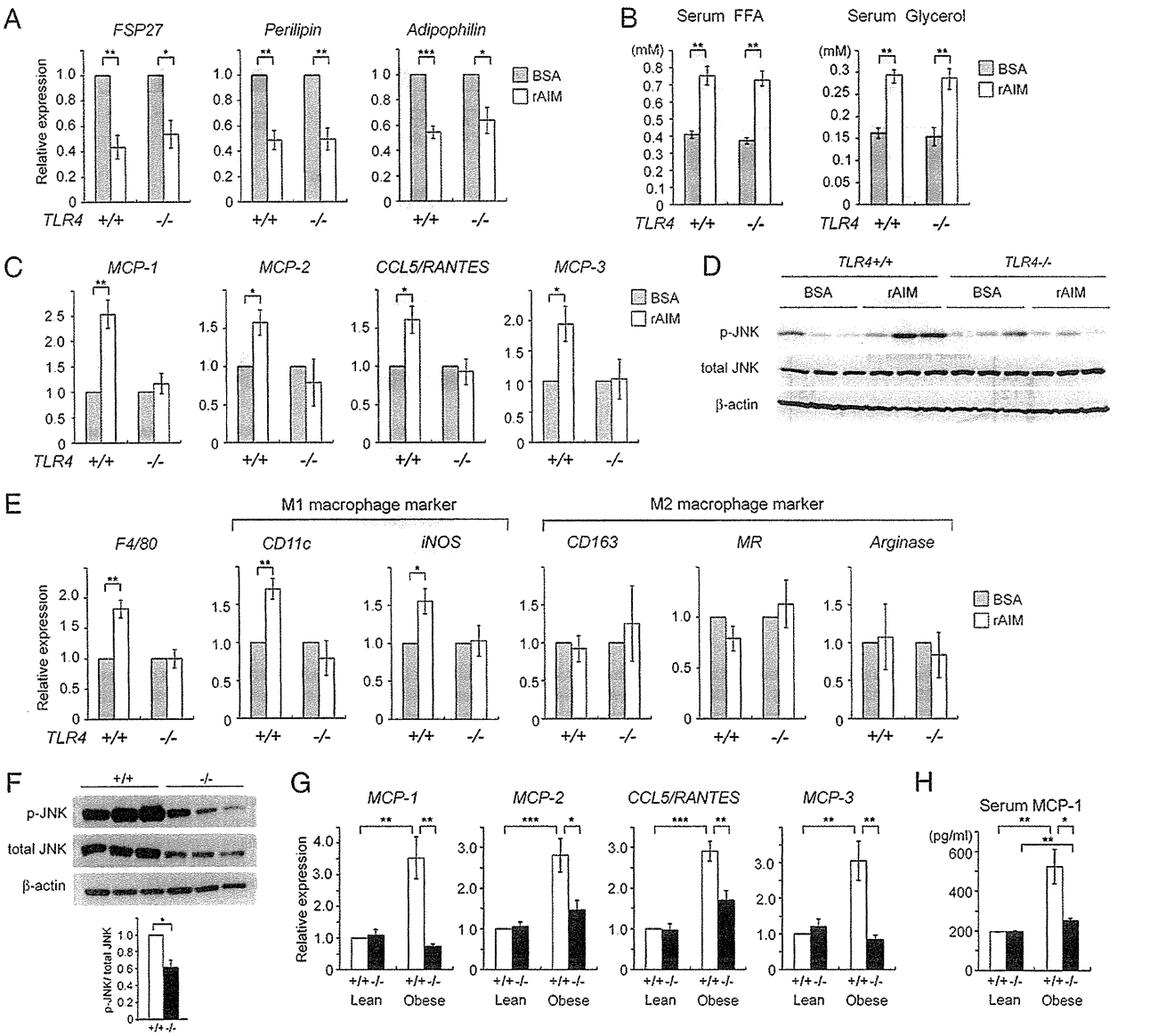

Fig. 3. Involvement of TLR4 in adipose tissue macrophage recruitment by AIM in vivo. (*A–E*) *TLR4*$^{-/-}$ and wild-type littermate mice (B6 background) were i.v. injected with rAIM or BSA three times every other day (400 μg in 200 μL PBS per injection). The day after the third injection (day 8 from the first injection), mice were killed, and lipolysis, chemokine expression, and adipose tissue macrophage accumulation were analyzed. $n = 5$ for each. (*A*) mRNA levels for *FSP27*, *Perilipin*, and *Adipophilin* were assessed by QPCR using RNA isolated from epididymal fat. Values were presented as relative expression to those of fat tissue injected with BSA. Error bar: SEM. (*B*) Serum levels for FFA and glycerol. (*C*) mRNA levels for chemokines. (*D*) Immunoblotting for total and phosphorylated JNK in epididymal fat. Immunoblot for β-actin is also presented. Results from three mice for each group are presented. Note that comparable results were obtained in five independent mice in each group. (*E*) mRNA levels for F4/80 pan-macrophage marker, M1 and M2 macrophage markers to assess macrophage recruitment. (*F*) Immunoblotting for total and phosphorylated JNK using lysates obtained from epididymal fats of *AIM*$^{+/+}$ and *AIM*$^{-/-}$ mice fed a HFD for 12 wk ($n = 4–6$). Relative values of phosphorylated JNK signals to total JNK are also presented (*Lower* graph). (*G*) QPCR analysis of mRNA levels for chemokine genes in epididymal fat tissue and (*H*) serum MCP-1 concentration in *AIM*$^{+/+}$ and *AIM*$^{-/-}$ mice fed a HFD for 0 (lean) or 12 wk (obese); $n = 6–8$.

Involvement of TLR4. As TIRAP is downstream of not only TLR4 but also other TLRs, including TLR2 (32), the precise involvement of TLR4 in macrophage recruitment was further verified. We first suppressed *TLR4* expression by siRNA in 3T3-L1 adipocytes and assessed the induction of MCP-1 by AIM CM. As shown in Fig. S6 *A–C*, induction of both mRNA and protein of MCP-1 by AIM CM was significantly reduced in cells transfected with siRNA for *TLR4*. In addition, we injected rAIM i.v. into wild-type and $TLR4^{-/-}$ mice and thereafter assessed the state of lipolysis and chemokine production in epididymal adipose tissue. In both types of mice, the mRNA levels of *FSP27* (also called *Cidec*), *Perilipin*, and *Adipophilin*, coating elements for lipid droplets, were decreased after challenging with rAIM (Fig. 3*A*), a finding consistent with the progression of lipolysis reported previously (17, 33, 34). Similarly, the increase in blood FFA and glycerol levels was equivalent in $TLR4^{-/-}$ and wild-type mice (Fig. 3*B*). In contrast, induction of mRNA for chemokines by rAIM injection was significantly less efficient in $TLR4^{-/-}$ than in wild-type mice (Fig. 3*C*). In line with this, phosphorylation levels of c-Jun N-terminal kinases (JNKs) in epididymal fat, which represent the state of TLR activation, were up-regulated in wild-type mice but not in $TLR4^{-/-}$ mice (Fig. 3*D*). Furthermore, the rAIM injection increased mRNA levels for M1 macrophage markers in epididymal adipose tissue of wild-type but not $TLR4^{-/-}$ mice, demonstrating that AIM-induced lipolysis could not recruit inflammatory macrophages into adipose tissue in the absence of TLR4 (Fig. 3*E*). There was no significant change in mRNA levels for M2 macrophage markers in both $TLR4^{-/-}$ and wild-type mice (Fig. 3*E*). Histological analysis revealed the presence of IL-6 expressing M1 macrophages after the rAIM injection in epididymal adipose tissue of wild-type mice but not of $TLR4^{-/-}$ mice (Fig. S6*D*).

Consistent results were obtained in obese $AIM^{+/+}$ and $AIM^{-/-}$ mice after 12 wk on a HFD. In epididymal fat, phosphorylation levels of JNKs were decreased in $AIM^{-/-}$ mice compared with $AIM^{+/+}$ mice (Fig. 3*F*). In addition, chemokine mRNA levels were also lower in $AIM^{-/-}$ than in $AIM^{+/+}$ adipose tissue (Fig. 3*G*). Moreover, the serum level of MCP-1 was lower in $AIM^{-/-}$ than in $AIM^{+/+}$ mice (Fig. 3*H*).

It is possible that fatty acids effluxed from adipocytes may stimulate TLR4 expressed not only on adipocytes but also on resident M2 macrophages within adipose tissue in a paracrine fashion and may induce chemokine expression in macrophages. To assess this possibility, we stained epididymal fat from wild-type $AIM^{+/+}$ mice fed a HFD for 6 wk for MR, a M2 macrophage marker, and MCP-1. As shown in Fig. S7, both adipocytes and M2 macrophages stained positive for MCP-1. As expected, in $AIM^{-/-}$ mice, neither adipocytes nor resident macrophages showed obvious MCP-1 expression. Thus, in summary, AIM-induced lipolysis provoked the efflux of saturated fatty acids, including palmitic and stearic acids, from adipocytes, and these fatty acids stimulated chemokine production in both adipocytes and resident macrophages via TLR4 activation, resulting in M1 macrophage migration.

Prevention of Obesity-Associated Inflammation and Insulin Resistance in $AIM^{-/-}$ Mice. As a consequence of abolished infiltration of inflammatory macrophages, the progression of obesity-associated inflammation was prevented both locally and systemically in obese $AIM^{-/-}$ mice. In adipose tissue (Fig. 4*A*) and the liver (Fig. S8), mRNA levels for proinflammatory cytokines, such as *TNFα*, *IL-6*, and *IL-1β*, were significantly lower in $AIM^{-/-}$ than in $AIM^{+/+}$ mice after a HFD for 12 wk. Consistent with this finding, serum levels of TNFα and IL-6 were lower in $AIM^{-/-}$ mice compared with $AIM^{+/+}$ mice (Fig. 4*B*).

Having observed decreased inflammation in $AIM^{-/-}$ mice, we next assessed insulin sensitivity in $AIM^{-/-}$ and $AIM^{+/+}$ mice fed a HFD for 12 wk. Activation of the insulin signaling pathway after i.v. injection of insulin was studied in adipose tissue, skeletal muscle (gastrocnemius), and liver. As shown in Fig. 4*C*, substantial insulin-stimulated phosphorylation of AKT and GSK3β protein kinases

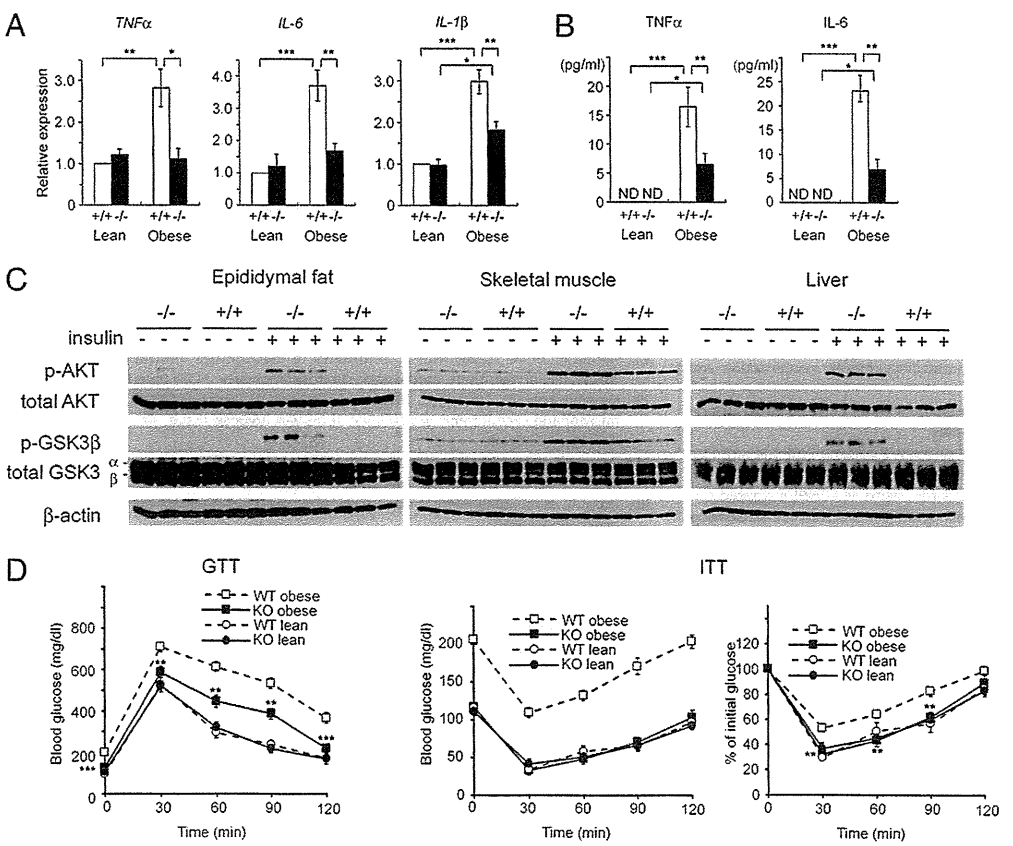

Fig. 4. Prevented inflammation and normal insulin sensitivity in obese $AIM^{-/-}$ mice. (*A*) Local inflammation. QPCR analysis of mRNA levels for inflammatory cytokine genes in epididymal fat tissue from $AIM^{+/+}$ or $AIM^{-/-}$ mice fed a HFD for 0 (lean) or 12 wk (obese). n = 6–8 for each group. Values were presented as relative expression to that in lean $AIM^{+/+}$ mice. Error bar: SEM. (*B*) Systemic inflammation. Serum TNFα and IL-6 levels are the same as in *A*. (*C*) $AIM^{-/-}$ and $AIM^{+/+}$ mice fed a HFD for 12 wk (three mice for each) were fasted for 5 h and treated with insulin (10 U/kg body weight) via i.p. injection. Within 15 min, epididymal fat, skeletal muscle (gastrocnemius), and liver were isolated and examined by immunoblotting for phosphorylated AKT (p-AKT), total AKT, phosphorylated GSK3β (p-GSK3β), total GSK3 (α and β), and β-actin. (*D*) Glucose tolerance test (GTT) and insulin tolerance test (ITT) performed on $AIM^{+/+}$ and $AIM^{-/-}$ mice fed a HFD for 0 (lean) or 12 wk (obese); n = 6–8 for each group. For ITT, two panels including absolute blood glucose levels (*Left*) and % of the initial (time 0) glucose level (*Right*) are presented.

was observed in all three tissues in $AIM^{-/-}$ mice in contrast to the markedly diminished phosphorylation levels in $AIM^{+/+}$ mice. Thus, insulin sensitivity was preserved in obese $AIM^{-/-}$ mice. Consistent with these results, whole-body glucose intolerance and insulin resistance observed in $AIM^{+/+}$ mice were found to be ameliorated in $AIM^{-/-}$ mice by i.p. glucose and insulin tolerance tests (GTT and ITT, respectively; Fig. 4*D*). Insulin production in pancreatic β cells in response to glucose was comparable in $AIM^{-/-}$ and $AIM^{+/+}$ mice, as assessed in vivo (Fig. S8*B*) and in vitro using isolated pancreatic Langerhans islets (Fig. S8*C*).

Conclusion

The present results provide unique and important evidence regarding the role of AIM in the initiation of chronic inflammation that connects obesity and insulin resistance. Firstly, macrophage recruitment into obese adipose tissues requires AIM-induced lipolysis. Augmentation of blood AIM levels may induce vigorous lipolysis in obese adipose tissues, increasing local extracellular fatty acid concentration to a level sufficient for the stimulation of TLR4, which triggers chemokine production by adipocytes and macrophage recruitment (summarized in Fig. S9). Although we and others previously reported some related facts underlying this conclusion, which were observed in a number of different physiological and experimental conditions (12, 14, 21–33), we would like to emphasize that this study, which focused on AIM, has uniquely linked apparently independent elements to a process that occurs during the progression to obesity.

Secondly, adipocyte hypertrophy is not solely sufficient for the initiation of macrophage infiltration; an increase in blood AIM needs to be accompanied. In $AIM^{-/-}$ mice, although the level of AIM-independent lipolysis increases in line with adipocyte hypertrophy (14), it may not reach a level sufficient for macrophage recruitment (Fig. S9). Thirdly, within adipose tissue, crosstalk between macrophages and adipocytes establishes a vicious cycle that accelerates inflammation; saturated fatty acids brought about by lipolysis activate TLR4 to induce TNFα, which in turn activates the TNFα receptor to produce inflammatory cytokines/adipokines and chemokines (35). The end point of this response is further progression of inflammation, lipolysis, and macrophage recruitment. It is likely that via an increase in lipolysis, AIM may strengthen this crosstalk, further contributing to the progression of inflammation (Fig. S9).

Thus, this study might not only advance our knowledge about the events triggering obesity-associated inflammation, but also open a door to the development of next-generation antimetabolic therapies via suppression of AIM.

Materials and Methods

Mice. $AIM^{-/-}$ mice (13) had been backcrossed to C57BL/6 (B6) for 13 generations before used for experiments. HFD (HFD32, fat kcal: 60%) was purchased from CREA. $TLR4^{-/-}$ mice (36) were kindly provided from Drs. S. Akira (Osaka University, Osaka, Japan) and K. Miyake (The Institute of Medical Science, University of Tokyo, Tokyo, Japan). All mice were maintained under a specific pathogen free condition.

Statistical Analysis. A two-tailed Mann-Whitney test was used to calculate *P* values. $***P < 0.001$, $**P < 0.01$, $*P < 0.05$. Error bars: SEM.

Please see *SI Materials and Methods* for further details.

ACKNOWLEDGMENTS. We thank Genostaff Inc. for technical assistance in histology. This work was supported by Grants-in-Aid for Scientific Research (B) (Japan Society for the Promotion of Science), the Global Centers of Excellence (COE) Program (T.M.), Kanae Foundation for the Promotion of Medical Science, the Astellas Foundation for Research on Metabolic Disorders, and the Ono Medical Research Foundation (S.A.).

1. Hotamisligil GS, Shargill N-S, Spiegelman B-M (1993) Adipose expression of tumor necrosis factor-alpha: Direct role in obesity-linked insulin resistance. *Science* 259: 87–91.
2. Wellen KE, Hotamisligil GS (2003) Obesity-induced inflammatory changes in adipose tissue. *J Clin Invest* 112:1785–1788.
3. Arkan MC, et al. (2005) IKK-beta links inflammation to obesity-induced insulin resistance. *Nat Med* 11:191–198.
4. Shoelson SE, Lee J, Goldfine AB (2006) Inflammation and insulin resistance. *J Clin Invest* 116:1793–1801.
5. Weisberg SP, et al. (2003) Obesity is associated with macrophage accumulation in adipose tissue. *J Clin Invest* 112:1796–1808.
6. Xu H, et al. (2003) Chronic inflammation in fat plays a crucial role in the development of obesity-related insulin resistance. *J Clin Invest* 112:1821–1830.
7. Solinas G, et al. (2007) JNK1 in hematopoietically derived cells contributes to diet-induced inflammation and insulin resistance without affecting obesity. *Cell Metab* 6: 386–397.
8. Gordon S, Taylor PR (2005) Monocyte and macrophage heterogeneity. *Nat Rev Immunol* 5:953–964.
9. Lumeng CN, Bodzin JL, Saltiel AR (2007) Obesity induces a phenotypic switch in adipose tissue macrophage polarization. *J Clin Invest* 117:175–184.
10. Ozcan U, et al. (2004) Endoplasmic reticulum stress links obesity, insulin action, and type 2 diabetes. *Science* 306:457–461.
11. Kahn SE, Hull RL, Utzschneider KM (2006) Mechanisms linking obesity to insulin resistance and type 2 diabetes. *Nature* 444:840–846.
12. Kosteli A, et al. (2010) Weight loss and lipolysis promote a dynamic immune response in murine adipose tissue. *J Clin Invest* 120:3466–3479.
13. Miyazaki T, Hirokami Y, Matsuhashi N, Takatsuka H, Naito M (1999) Increased susceptibility of thymocytes to apoptosis in mice lacking AIM, a novel murine macrophage-derived soluble factor belonging to the scavenger receptor cysteine-rich domain superfamily. *J Exp Med* 189:413–422.
14. Kurokawa J, et al. (2010) Macrophage-derived AIM is endocytosed into adipocytes and decreases lipid droplets via inhibition of fatty acid synthase activity. *Cell Metab* 11:479–492.
15. Joseph SB, et al. (2004) LXR-dependent gene expression is important for macrophage survival and the innate immune response. *Cell* 119:299–309.
16. Valledor AF, et al. (2004) Activation of liver X receptors and retinoid X receptors prevents bacterial-induced macrophage apoptosis. *Proc Natl Acad Sci USA* 101: 17813–17818.
17. Gebe JA, et al. (1997) Molecular cloning, mapping to human chromosome 1 q21-q23, and cell binding characteristics of Spalpha, a new member of the scavenger receptor cysteine-rich (SRCR) family of proteins. *J Biol Chem* 272:6151–6158.
18. Kim WK, et al. (2008) Glycoproteomic analysis of plasma from patients with atopic dermatitis: CD5L and ApoE as potential biomarkers. *Exp Mol Med* 40:677–685.
19. Gray J, et al. (2009) A proteomic strategy to identify novel serum biomarkers for liver cirrhosis and hepatocellular cancer in individuals with fatty liver disease. *BMC Cancer* 9:271.
20. Arai S, et al. (2005) A role for the apoptosis inhibitory factor AIM/Spalpha/Api6 in atherosclerosis development. *Cell Metab* 1:201–213.
21. Shi H, et al. (2006) TLR4 links innate immunity and fatty acid-induced insulin resistance. *J Clin Invest* 116:3015–3025.
22. Suganami T, et al. (2007) Role of the Toll-like receptor 4/NF-kappaB pathway in saturated fatty acid-induced inflammatory changes in the interaction between adipocytes and macrophages. *Arterioscler Thromb Vasc Biol* 27:84–91.
23. Poggi M, et al. (2007) C3H/HeJ mice carrying a toll-like receptor 4 mutation are protected against the development of insulin resistance in white adipose tissue in response to a high-fat diet. *Diabetologia* 50:1267–1276.
24. Tsukumo DM, et al. (2007) Loss-of-function mutation in Toll-like receptor 4 prevents diet-induced obesity and insulin resistance. *Diabetes* 56:1986–1998.
25. Davis JE, Gabler NK, Walker-Daniels J, Spurlock ME (2008) Tlr-4 deficiency selectively protects against obesity induced by diets high in saturated fat. *Obesity (Silver Spring)* 16:1248–1255.
26. Kamei N, et al. (2006) Overexpression of monocyte chemoattractant protein-1 in adipose tissues causes macrophage recruitment and insulin resistance. *J Biol Chem* 281:26602–26614.
27. Kanda H, et al. (2006) MCP-1 contributes to macrophage infiltration into adipose tissue, insulin resistance, and hepatic steatosis in obesity. *J Clin Invest* 116:1494–1505.
28. Keophiphath M, Rouault C, Divoux A, Clément K, Lacasa D (2010) CCL5 promotes macrophage recruitment and survival in human adipose tissue. *Arterioscler Thromb Vasc Biol* 30:39–45.
29. Soma MR, Mims MP, Chari MV, Rees D, Morrisett JD (1992) Triglyceride metabolism in 3T3-L1 cells. An in vivo 13C NMR study. *J Biol Chem* 267:11168–11175.
30. Kopp A, et al. (2009) Fatty acids as metabolic mediators in innate immunity. *Eur J Clin Invest* 39:924–933.
31. Schaeffler A, et al. (2009) Fatty acid-induced induction of Toll-like receptor-4/nuclear factor-kappaB pathway in adipocytes links nutritional signalling with innate immunity. *Immunology* 126:233–245.
32. Jenkins KA, Mansell A (2010) TIR-containing adaptors in Toll-like receptor signalling. *Cytokine* 49:237–244.
33. Zechner R, Strauss JG, Haemmerle G, Lass A, Zimmermann R (2005) Lipolysis: Pathway under construction. *Curr Opin Lipidol* 16:333–340.
34. Nishino N, et al. (2008) FSP27 contributes to efficient energy storage in murine white adipocytes by promoting the formation of unilocular lipid droplets. *J Clin Invest* 118: 2693–2696.
35. Schäffler A, Schölmerich J, Salzberger B (2007) Adipose tissue as an immunological organ: Toll-like receptors, C1q/TNFs and CTRPs. *Trends Immunol* 28:393–399.
36. Hoshino K, et al. (1999) Cutting edge: Toll-like receptor 4 (TLR4)-deficient mice are hyporesponsive to lipopolysaccharide: Evidence for TLR4 as the Lps gene product. *J Immunol* 162:3749–3752.

Death effector domain–containing protein (DEDD) is required for uterine decidualization during early pregnancy in mice

Mayumi Mori,[1] Miwako Kitazume,[1] Rui Ose,[2] Jun Kurokawa,[1] Kaori Koga,[3] Yutaka Osuga,[3] Satoko Arai,[1] and Toru Miyazaki[1]

[1]Laboratory of Molecular Biomedicine for Pathogenesis, Center for Disease Biology and Integrative Medicine, Faculty of Medicine, The University of Tokyo, Bunkyo-ku, Tokyo, Japan. [2]Department of Human Genome Research, Kazusa DNA Research Institute, Kisarazu, Chiba, Japan. [3]Department of Obstetrics and Gynecology, Faculty of Medicine, The University of Tokyo, Bunkyo-ku, Tokyo, Japan.

During intrauterine life, the mammalian embryo survives via its physical connection to the mother. The uterine decidua, which differentiates from stromal cells after implantation in a process known as decidualization, plays essential roles in supporting embryonic growth before establishment of the placenta. Here we show that female mice lacking death effector domain–containing protein (DEDD) are infertile owing to unsuccessful decidualization. In uteri of *Dedd*$^{-/-}$ mice, development of the decidual zone and the surrounding edema after embryonic implantation was defective. This was subsequently accompanied by disintegration of implantation site structure, leading to embryonic death before placentation. Polyploidization, a hallmark of mature decidual cells, was attenuated in DEDD-deficient cells during decidualization. Such inefficient decidualization appeared to be caused by decreased Akt levels, since polyploidization was restored in DEDD-deficient decidual cells by overexpression of Akt. In addition, we showed that DEDD associates with and stabilizes cyclin D3, an important element in polyploidization, and that overexpression of cyclin D3 in DEDD-deficient cells improved polyploidization. These results indicate that DEDD is indispensable for the establishment of an adequate uterine environment to support early pregnancy in mice.

Introduction

Approximately 10%–15% of couples experience infertility during their reproductive years, owing mainly to implantation failure. Among the reasons underlying such failure, defective development of functional decidua at the implantation site within the uterus has recently been highlighted (1–3). In response to implantation, stromal cells immediately surrounding the mucosal crypt where the embryo is embedded proliferate extensively and undergo differentiation into polyploid decidual cells, forming an avascular primary decidual zone, followed by a broad, well-vascularized secondary decidual zone. It is believed that this decidual structure is important for the provision of nutrition to the developing embryo and also acts as a barrier against uncontrolled trophoblast proliferation until the placenta develops. Analyses of mutant mice that show female infertility, such as in knockout mice for homeobox A10 (*Hoxa10*) (4, 5) or IL-11 receptor (6), have contributed to the investigation of the molecular mechanisms involved in decidualization. Recent evidence has implicated cell-cycle regulation as being essential for both the proliferation and differentiation of stromal cells. In particular, Das and colleagues reported that cyclin D3–dependent activation of cyclin-dependent kinase 4 (Cdk4) or Cdk6 appears to be involved sequentially in those two events during decidua formation (7). In addition to these essential elements, in this report, we present data indicating that the death effector domain–containing (DED-containing) protein DEDD is indispensable for the maturation of decidual cells and support of female fertility in mice.

We previously found that the DEDD protein, initially described as a member of the DED-containing protein family, is associated with the Cdk1/cyclin B1 complex, thereby decreasing the kinase activity of Cdk1 (8). This response impedes Cdk1-dependent mitotic progression, preserving synthesis of ribosomal RNA (rRNA) and protein and resulting in sufficient cell growth before cell division (8, 9). Consistently, depletion of DEDD results in a shortened mitotic duration, an overall decrease in the amount of cellular rRNA and protein, and decreased cell and body size (8, 9). In addition to the function of DEDD as a cell-cycle regulator, we recently determined that DEDD associates with S6K1 (10) and Akt (11), major elements of the signaling cascade involving mitogen-related PI3K. Such associations support the roles of S6K1 activity and Akt protein stability, respectively, in contributing to the maintenance of glucose homeostasis in the body (10, 11). Hence, DEDD is multifunctional and is involved in different physiological mechanisms. In fact, we found that female *Dedd*$^{-/-}$ mice are infertile, and embryos of all DEDD genotypes die during early pregnancy within the *Dedd*$^{-/-}$ uterus, whereas *S6K1*$^{-/-}$ female mice, which also show a similar small phenotype and attenuated glucose homeostasis, show normal fertility (12). Given the phenotypic similarity of *Dedd*$^{-/-}$ mice to other infertile mutant mice (4–6), this observation led us to address whether DEDD might also be involved in uterine decidualization.

In the present study, we assessed embryos implanted in *Dedd*$^{-/-}$ uteri. In addition, we analyzed the maturation state of uterine decidual cells from *Dedd*$^{-/-}$ mice in vitro and in vivo. We also studied the molecular mechanism underlying the inefficient decidualization of *Dedd*$^{-/-}$ cells.

Results

Female Dedd$^{-/-}$ *mice are infertile.* We found that *Dedd*$^{-/-}$ female mice exhibited complete sterility when mated with males of any genotype (*Dedd*$^{-/-}$, *Dedd*$^{+/-}$, or *Dedd*$^{+/+}$), although *Dedd*$^{-/-}$ offspring were born from the intercross of *Dedd*$^{+/-}$ mice at a Mendelian ratio, and

Conflict of interest: The authors have declared that no conflict of interest exists.
Citation for this article: *J Clin Invest.* 2011;121(1):318–327. doi:10.1172/JCI44723.

Table 1
Female *Dedd*$^{-/-}$ mice are infertile

Genotype		Offspring					
Female	Male	+/+	+/–	–/–	Sum	*n*	Birth rate
+/+	+/–	13 (46%)	15 (54%)	0 (0%)	28	6	4.67
+/+	–/–	0 (0%)	87 (100%)	0 (0%)	87	18	4.83
+/–	+/+	24 (51%)	23 (49%)	0 (0%)	47	10	4.70
+/–	+/–	108 (30%)	183 (51%)	66 (19%)	357	65	5.49
+/–	–/–	0 (0%)	47 (64%)	27 (36%)	74	17	4.35
–/–	+/+	0	0	0	0	23	0.00
–/–	+/–	0	0	0	0	37	0.00
–/–	–/–	0	0	0	0	12	0.00

The breeding efficiency in male-female combinations of various DEDD genotypes was investigated. Sum, total number of newborns; *n*, number of successful matings (with a vaginal plug); birth rate: sum/*n*.

Dedd$^{-/-}$ male mice were fertile (Table 1). Mating efficiency was comparable in female *Dedd*$^{-/-}$ mice and female mice of other genotypes, as assessed by vaginal plug formation (data not shown). The uterine *Dedd* mRNA level was upregulated after 4.5 dpc as assessed by quantitative RT-PCR (QPCR) (Figure 1A). An increase in *Dedd* expression was also observed in stromal cells differentiated to mature decidual cells in vitro in the presence of estrogen, progesterone (P4), and heparin-binding EGF-like growth factor (HB-EGF) (Figure 1B). Upregulation of *DEDD* expression along with the decidualization was also detected in human uterine stromal cells (Figure 1C). These results suggested that uterine DEDD is important after implantation and that the maturation of uterine decidual cells may be associated with DEDD expression.

Consistently, when 4.5-dpc uteri were analyzed with injection of blue dye (1% Chicago blue solution) (13), the number of implantation sites was comparable in *Dedd*$^{-/-}$ and *Dedd*$^{+/+}$ mice (6.8 ± 0.73 in *Dedd*$^{-/-}$ mice and 7.4 ± 0.40 in *Dedd*$^{+/+}$ mice; $n = 5$ each). In addition, the spacing and crowding of implanted embryos in the uterus was also similar in *Dedd*$^{-/-}$ and *Dedd*$^{+/+}$ mice (Figure 1D). Histologic analysis of 4.5-dpc *Dedd*$^{-/-}$ uteri revealed normal embryonic implantation (Figure 1E). No difference was observed in the size of the edematous region and the decidual zone, which are formed in response to implantation (Figure 1E). Immunostaining for COX-2, an implantation site marker (14), corroborated the finding of normal embryonic implantation in *Dedd*$^{-/-}$ and *Dedd*$^{+/+}$ uteri (Figure 1E). Similarly, the mRNA level for *Ptgs2/Cox2* was comparable in *Dedd*$^{-/-}$ and *Dedd*$^{+/+}$ uteri, as assessed by QPCR with total RNA isolated from implantation sites (data not shown). However, anatomical analysis showed that in *Dedd*$^{-/-}$ uteri, the number of living embryos decreased rapidly between 5.5 and 8.5 dpc (Figure 1F). At 9.5 dpc, the period of placenta formation, no living embryos were detected in *Dedd*$^{-/-}$ uteri (Figure 1F). During this period, living embryos in *Dedd*$^{-/-}$ uteri were of smaller size compared with those in *Dedd*$^{+/+}$ uteri, and the difference in average embryo size between these two groups became more prominent at later dpc (Table 2). Thus, whereas implantation occurred normally in *Dedd*$^{-/-}$ uteri, embryos showed growth defects and died by 9.5 dpc, before placenta formation. Note that serum levels of estrogen and P4, as well as mRNA levels for the receptor for each hormone (*Esr1* and *Pgr*, respectively) were similar in *Dedd*$^{-/-}$ and *Dedd*$^{+/+}$ females (Supplemental Figure 1; supplemental material available online with this article; doi:10.1172/JCI44723DS1). Preimplantation uterine histology was also comparable (Supplemental Figure 2). In addition, the proliferation of uterine epithelial and stromal cells as well as expression induction of genes such as *Vegf* and *Lif* in response to estrogen were similar in *Dedd*$^{-/-}$ and *Dedd*$^{+/+}$ ovariectomized mice (Supplemental Figure 3). In addition, histologic ovarian morphology, ovulation, and intrauterine fertilization were normal in *Dedd*$^{-/-}$ females (data not shown).

Defective decidualization and disintegrated structure of the implantation site in Dedd$^{-/-}$ *uteri.* Histological analysis of 5.5-dpc uteri showed that the size of the decidual zone was smaller in *Dedd*$^{-/-}$ compared with *Dedd*$^{+/+}$ mice (Figure 2A). This was confirmed by immunostaining for the decidua marker tissue inhibitor of metalloproteinase 3 (TIMP3) (quantification also shown in Figure 2A) (15). Consistent with these results, mRNA levels for various genes that are highly expressed in decidual cells were decreased in *Dedd*$^{-/-}$ compared with *Dedd*$^{+/+}$ uteri, as assessed by QPCR with total RNA isolated from implantation sites (Figure 2B). Of these, the expression level of P4-sensitive bone morphogenetic protein 2 (*Bmp2*) gene was compromised at 5.5 d.p.c in *Dedd*$^{-/-}$ uteri, whereas that of *Hoxa10*, upstream of *Bmp2* (5, 16, 17), was similar to that in *Dedd*$^{+/+}$ uteri. In addition to the decidual zone, the size of the edematous region surrounding the decidual zone was also decreased in *Dedd*$^{-/-}$ compared with *Dedd*$^{+/+}$ mice (Figure 2A), suggesting that vascular permeability might be reduced in *Dedd*$^{-/-}$ uteri.

Such attenuated development of the decidual zone in *Dedd*$^{-/-}$ uteri was accompanied by disintegrated structure of the implantation site at later phases of pregnancy. At 7.5 dpc, a large proportion of decidual cells exhibited a shrunken shape, and marked bleeding was detected at the edge of the cavity in *Dedd*$^{-/-}$ uteri (Figure 2C). In 8.5-dpc *Dedd*$^{-/-}$ uteri, the structure of the outer wall of the embryonic cavity, which is supported by Reichert's membrane and trophoblastic giant cells (TGCs), had collapsed (Figure 2C), and irregular distribution of TGCs (i.e., invasion of TGCs into inner area of uteri) was more remarkable (Figure 2D). Such inadequate uterine environment may cause infertility in female *Dedd*$^{-/-}$ mice.

Defective polyploidy in Dedd$^{-/-}$ *decidual cells.* We next assessed the state of polyploidy, a hallmark of mature decidual cells, in *Dedd*$^{-/-}$ and *Dedd*$^{+/+}$ uterine stromal cells undergoing decidualization in vitro in the presence of estrogen, P4, and HB-EGF. As shown in Figure 3A, at days 3 and 7, the proportion of multinuclear cells observed microscopically was more than 50% smaller in *Dedd*$^{-/-}$ cells than in *Dedd*$^{+/+}$ cells. Consistent with this result, analysis of these cells by the flow cytometer after DNA staining revealed a significant decrease in the proportion of cells that possessed more than 4 copies of genomic DNA (indicated as 4n and 8n) in *Dedd*$^{-/-}$ compared with *Dedd*$^{+/+}$ cells (Figure 3B). Similar results were obtained in vivo in cells isolated from 4.5-dpc implantation sites in *Dedd*$^{-/-}$ and *Dedd*$^{+/+}$ uteri by collagenase treatment (Figure 3C). Thus, the defect in decidualization observed in *Dedd*$^{-/-}$ uteri was associated with attenuated terminal maturation with less polyploidy.

In contrast, the proliferative status of uterine stromal cells in response to implantation was not different in *Dedd*$^{-/-}$ and *Dedd*$^{+/+}$ mice, as judged by the comparable cell number isolated from implantation sites at 4.5 dpc ($1.08 \times 10^6 \pm 0.15 \times 10^6$ in *Dedd*$^{-/-}$

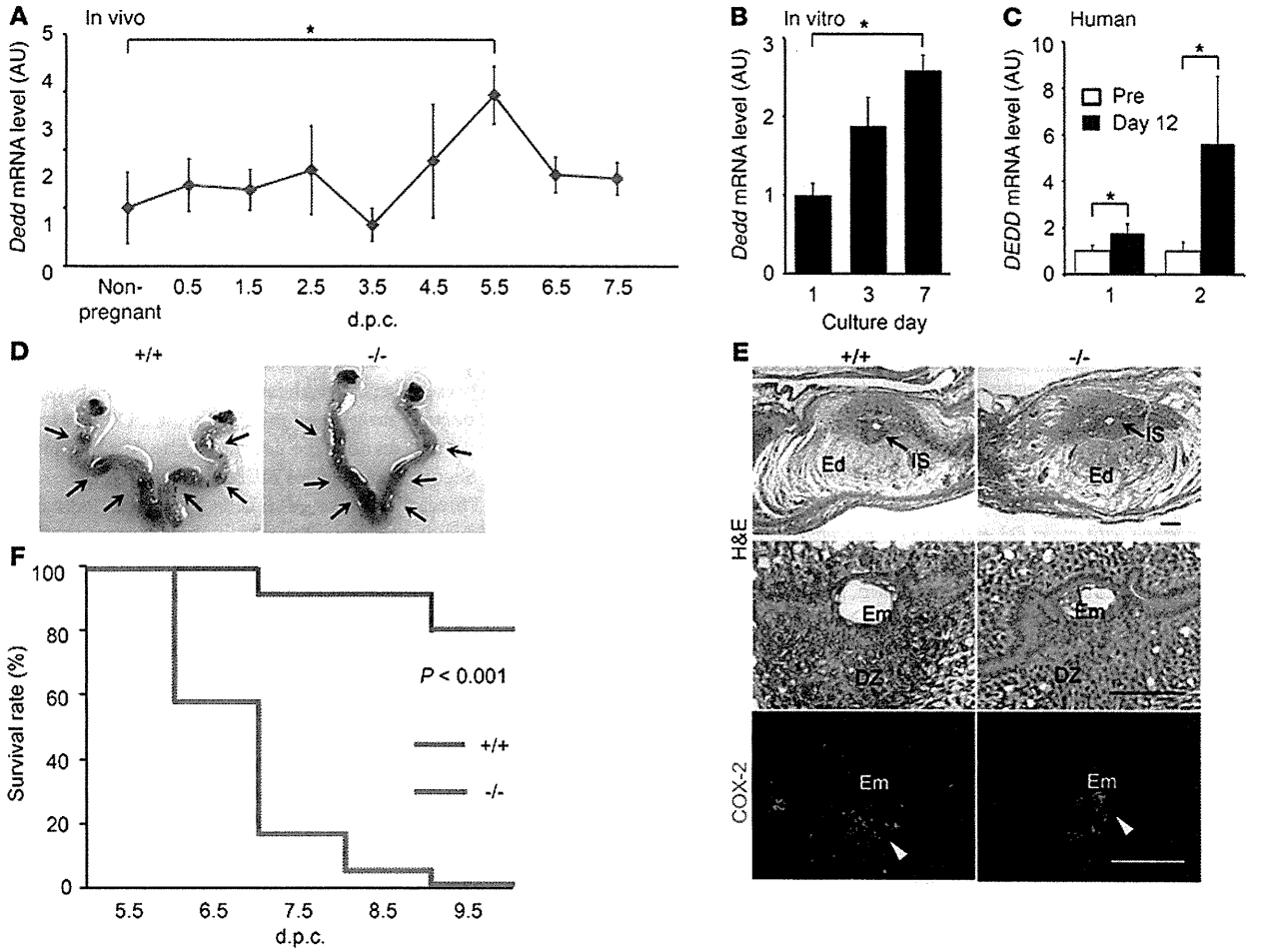

Figure 1

Postimplantation embryonic death in *Dedd*$^{-/-}$ uteri. (**A–C**) Increase in *Dedd* mRNA level in response to implantation in wild-type mouse (**A**) or in vitro decidualization in mouse uterine stromal (**B**) and human endometrial (**C**) cells, assessed by QPCR. Values were normalized to those of β-*actin* or *GAPDH* and are presented as relative expression to those of nonpregnant (**A**), day 1 (**B**), or undifferentiated (**C**) controls. Pre, undifferentiated cells; Day 12, decidualized cells at 12 days after the differentiation induction. In **C**, results from triplicate experiments using specimens from two individuals (1 and 2) are shown. Error bars indicate SEM. (**D**) Embryo spacing and crowding were assessed by blue dye injection. Representative photos of the uteri are shown. (**E**) Histologic analysis of implantation sites at 4.5 dpc in *Dedd*$^{+/+}$ (+/+) and *Dedd*$^{-/-}$ (–/–) uteri. Sections were stained with H&E or immunostained for COX-2. Em, embryo; DZ, decidual zone; Ed, edematous region (outside of DZ, white zone). Positive signals for COX-2 are indicated by arrowheads. Scale bars: 200 μm. (**F**) Survival rates of embryos during early gestation (Kaplan-Meier method). When embryo bodies were observed, regardless of size, they were regarded as "alive," whereas degenerated masses or those with scars at implantation sites were regarded as "dead." $n = 75$ for *Dedd*$^{+/+}$ and $n = 44$ for *Dedd*$^{-/-}$ uteri; log-rank, $\chi^2 = 13.2$. $^*P < 0.05$.

mice and $1.21 \times 10^6 \pm 0.075 \times 10^6$ in *Dedd*$^{+/+}$ mice; $n = 3$ each). Consistent with this result, when decidualizing stromal cells were challenged in vitro with 5-ethynil-2′-deoxyuridine (EdU; a nucleotide analog of thymidine), the proportion of EdU-incorporated cells was equivalent in *Dedd*$^{-/-}$ and *Dedd*$^{+/+}$ cells (Supplemental Figure 4A). Also, in vivo, 5.5-dpc implantation sites in *Dedd*$^{-/-}$ and *Dedd*$^{+/+}$ uteri stained similarly for Ki67, which identifies proliferating cells (Supplemental Figure 4B).

Decreased Akt level in Dedd$^{-/-}$ *uteri and increase in polyploidy by Akt expression in Dedd*$^{-/-}$ *decidual cells.* As we reported previously, the amount of Akt (all isotypes) is decreased in various *Dedd*$^{-/-}$ tissues, owing to decreased Akt protein stability (11). Notably, implantation sites in 5.5-dpc *Dedd*$^{-/-}$ uteri also showed decreased levels of Akt protein compared with those in *Dedd*$^{+/+}$ uteri, as assessed by immunoblotting with a pan-Akt antibody (Figure 4A). Parallel results were also obtained using in vitro decidualizing cells (Supplemental Figure 5). Signal for activated Akt phosphorylated at Thr308 was also decreased (Figure 4A, p-Akt). As we observed in mouse embryonic fibroblasts (MEFs) and other tissues (11), mRNA levels for *Akt1* and *Akt2* did not decrease in these cells (data not shown). To test whether the decrease in Akt protein was essential for the defect in polyploidy observed in *Dedd*$^{-/-}$ decidual cells (Figure 3), Akt-1 was overexpressed in in vitro differentiating *Dedd*$^{-/-}$ uterine stromal cells, and polyploidy was analyzed. As expected, the proportion of polynuclear cells was significantly increased by forced Akt-1 expression (Figure 4B). Thus, a decrease in Akt protein level appeared to be responsible for the inefficient decidualization observed in *Dedd*$^{-/-}$ uteri.

Table 2
Embryo size within *Dedd*$^{+/+}$ and *Dedd*$^{-/-}$ uteri

	Maternal genotype	Embryo size (mm^3)	*n*
Day 5.5	+/+	0.0059 ± 0.0014	9
	–/–	0.0039 ± 0.0012^A	9
Day 6.5	+/+	0.17 ± 0.014	5
	–/–	0.044 ± 0.0096^B	12
Day 7.5	+/+	0.51 ± 0.070	19
	–/–	0.25 ± 0.099^A	11
Day 8.5	+/+	>5.00	11
	–/–	1.00 ± 0.33	7

Both *Dedd*$^{+/+}$ (+/+) females and *Dedd*$^{-/-}$ (–/–) females were mated with *Dedd*$^{+/+}$ males. Therefore, embryos in *Dedd*$^{+/+}$ uteri were either *Dedd*$^{+/-}$ or *Dedd*$^{+/+}$, whereas those in *Dedd*$^{-/-}$ uteri were all *Dedd*$^{+/-}$. There was no significant difference in the size among the *Dedd*$^{+/-}$ and *Dedd*$^{+/+}$ embryos in *Dedd*$^{+/+}$ uteri. $^AP < 0.05$, $^BP < 0.001$.

Dedd associates with cyclin D3 and supports its protein stability. Of the multiple functions of Akt, control of the cell cycle via regulation of D-type cyclins in terms of gene expression, protein stability, and localization within the cell has been documented in different physiologic and pathologic situations (18). Das and colleagues recently implicated cyclin D3 as a key regulator of polynuclearization (7, 19, 20). In addition, García-Morales et al. showed that the protein stability of cyclin D3 is downregulated by rapamycin, an inhibitor of mammalian target of rapamycin (mTOR), downstream of Akt in the PI3K signaling pathway (21). This suggests that the decrease in Akt protein in the absence of DEDD might influence cyclin D3, resulting in a defect in polyploidy. To test this, we stained *Dedd*$^{-/-}$ and *Dedd*$^{+/+}$ uteri for cyclin D3 at 5.5 dpc. As shown in Figure 5A, *Dedd*$^{-/-}$ decidua harbored fewer cyclin D3–positive cells. This decrease in cyclin D3 was confirmed by immunoblotting (Figure 5B). However, the mRNA level for cyclin D3 was similar in *Dedd*$^{-/-}$ and *Dedd*$^{+/+}$ uteri at 5.5 d.p.c (Figure 5C), suggesting that the stability of cyclin D3 is affected in *Dedd*$^{-/-}$ cells. Therefore, we measured the half-life of cyclin D3 protein in in vitro differentiating stromal cells at day 3. Importantly, the amount of cyclin D3 protein started to decrease within 30 minutes in *Dedd*$^{-/-}$ cells but not in *Dedd*$^{+/+}$ cells (Figure 5D). By 90 minutes, the protein level of cyclin D3 was more than 3-fold lower in *Dedd*$^{-/-}$ compared with *Dedd*$^{+/+}$ cells (Figure 5D). The presence of MG132, a proteasome inhibitor, tempered the decrease observed in *Dedd*$^{-/-}$ cells (Figure 5D). Thus, lack of DEDD resulted in instability of cyclin D3. As in the case of Akt, increase in cyclin D3 protein by overexpression improved polyploidy in *Dedd*$^{-/-}$ decidual cells (Figure 5E), indicating that a decrease in cyclin D3 protein level also appeared to be involved in the inefficient decidualization observed in *Dedd*$^{-/-}$ uteri.

Such a relationship among DEDD, cyclin D3, and Akt was also supported by an in situ mRNA analysis using 5.5- and 7.5-dpc *Dedd*$^{+/+}$ uteri, which demonstrated coexpression of these 3 genes at the decidual zone cells in vivo (Figure 6A). Furthermore, DEDD associated with cyclin D3. This is similar to our previous observations that DEDD binds to various proteins such as cyclin B1, S6K1, and Akt (8–11). As shown in Figure 6B, immunoprecipitation in HEK293T cells expressing both FLAG-tagged cyclin D3 and hemagglutinin-tagged (HA-tagged) DEDD showed that the two proteins coprecipitated, indicating that DEDD may facilitate a complex with cyclin D3. Therefore, DEDD might support the stability of cyclin D3 by two independent pathways: maintenance of the Akt protein level and direct formation of a DEDD/cyclin D3 complex. HA-tagged DEDD also coprecipitated with FLAG-tagged Cdk4 and Cdk6 (Figure 6B). Endogenous DEDD was also coprecipitated with cyclin D3, Cdk4, or Cdk6, when tested using protein isolated from implantation sites of 5.5-dpc uteri (Figure 6C). Similar to our observation that DEDD associates with Cdk1/cyclin B1 via direct binding to cyclin B1, DEDD might form a complex with Cdk4/cyclin D3 and Cdk6/cyclin D3, both of which are essential for the regulation of decidualization (9), via a direct association with cyclin D3.

Discussion

A new role for DEDD in uterine decidualization and female fertility. Results of the present study implicate DEDD as an indispensable element in supporting early pregnancy. First, DEDD was expressed in decidual cells, and its absence decreased the Akt protein level in these cells. Second, the lack of DEDD decreased the stability of cyclin D3. Third, *Dedd*$^{-/-}$ stromal cells showed defective polyploidy during decidualization. Fourth, in *Dedd*$^{-/-}$ uteri, inefficient polyploidy disturbed development of the decidual zone, which was accompanied by disintegrated structure of the implantation site. As a result of these defects, *Dedd*$^{-/-}$ uteri cannot support embryonic growth before the development of the placenta, resulting in complete infertility of *Dedd*$^{-/-}$ female mice.

The decidual cell polyploidy, which is a hallmark of mature decidual cells particularly in mice, is characterized by the formation of large mono- or binucleated cells, consisting of DNA with multiples of the haploid complement (22–24). Although it has been suggested that various biological processes including metabolic activity are associated with the polyploidy (25), the physiological significance of this event in uterine decidualization remains poorly understood. Complete infertility in female *Dedd*$^{-/-}$ mice whose decidua showed a normal proliferative activity but less polyploidy may suggest the functional importance of polyploidy for the support of embryonic growth during early pregnancy.

It could be argued that the general effect of DEDD deficiency, such as decreased body size and mild attenuation of insulin production (8–11), might cause infertility. However, this is unlikely, given that female *S6K1*$^{-/-}$ mice, which show a similar (or even more advanced) phenotype regarding body size and insulin production, remain fertile (12). Similarly, although *Akt1*$^{-/-}$ mice also showed fetal growth impairment due to placental inefficiency, adult females are fertile (26).

Association of DEDD with decidual polyploidy via support of Akt and cyclin D3 stability. One reason why the absence of DEDD causes infertility appears to be the decrease in the amount of Akt protein in uterine stromal/decidual cells. Recent evidence in humans and mice suggests that Akt may play a role in the regulation of decidualization and in the survival of decidual cells. Of note, Hirota et al. showed increased decidual polyploidy with upregulation of Akt phosphorylation in mice with deficiency for p53 restricted to the uterus (27). As we reported previously, DEDD forms a complex with Akt and heat shock protein 90 (Hsp90) and stabilizes all isoforms of Akt protein (11). It is possible that defective protein stability of cyclin D3 may be brought about, in part, by a decrease in Akt, based on the facts that D-type cyclins are substrates for Akt, cyclin D3 is regarded as a major regulator of polyploidy, and the deficient polyploidy observed in *Dedd*$^{-/-}$ cells was improved by forced expression of Akt-1. Nevertheless, the precise machinery whereby Akt influences the stability of cyclin D3 is not yet clear.

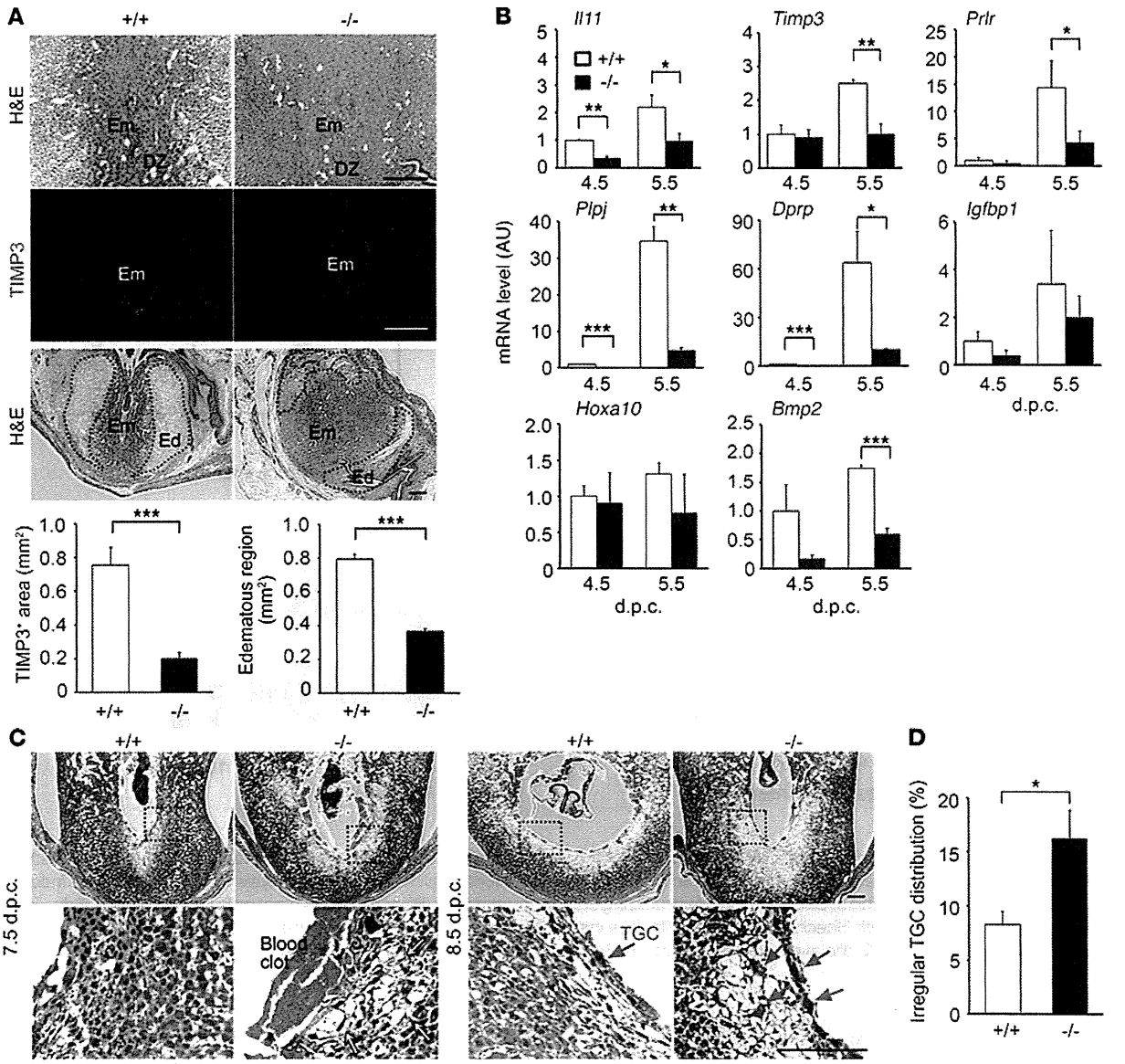

Figure 2

Defective decidualization in *Dedd*$^{-/-}$ uteri. (**A**) Implantation sites of 5.5-dpc *Dedd*$^{+/+}$ and *Dedd*$^{-/-}$ uteri were stained with H&E or immunostained for TIMP3. Scale bars: 200 μm. Quantification of decidual zone (TIMP3-positive area) and edematous region is also presented. At least 10 different sections in 3 different implantation sites were analyzed for each. Error bars indicate SEM. (**B**) mRNA levels of various genes that are highly expressed in decidua were analyzed by QPCR with total RNA isolated from 3 different implantation sites at 4.5 or 5.5 dpc. Values were normalized to those of β-*actin* and are presented as relative expression to 4.5-dpc *Dedd*$^{+/+}$ mice. Error bars indicate SEM. *Prlr*, prolactin receptor; *Plpj*, prolactin-like protein J; *Dprp*, decidual prolactin-related protein; *Igfbp1*, IGF-binding protein 1. (**C**) Histologic analysis of 7.5- and 8.5-dpc uteri (H&E staining). Higher magnification of the boxed area in the respective upper panel is presented in the lower panel. Arrows at 7.5 dpc indicate shrunken cells in *Dedd*$^{-/-}$ uterus. TGCs are denoted by blue arrows. Scale bars: 200 μm. (**D**) Irregular distribution of TGCs in *Dedd*$^{-/-}$ uterus. TGC numbers at the antimesometrial region of implantation sites were determined microscopically. At least 10 sections from 3 different specimens were examined. Data are shown as relative proportion of TGCs showing irregular distribution (invasion into the inner area). Error bars indicate SEM. $^{*}P < 0.05$, $^{**}P < 0.01$, $^{***}P < 0.001$.

Further studies are required to address the molecular mechanism. Interestingly, DEDD associates with cyclin D3; this might contribute structurally to the protein stability of cyclin D3.

Because cyclin D3–deficient mice do not show complete infertility, as observed in *Dedd*$^{-/-}$ mice (19, 28), a combination of various defects at the implantation site in addition to inefficient polyploidy — such as inadequate development of the edematous region (Figure 2A) and disintegrated structure of the implantation site at 7–8 d.p.c (Figure 2C) — might contribute to the overall infertility observed in *Dedd*$^{-/-}$ mice. These defects may also result from the decreased Akt level, given that Akt has diverse functions, including the maintenance of vascular permeability and an

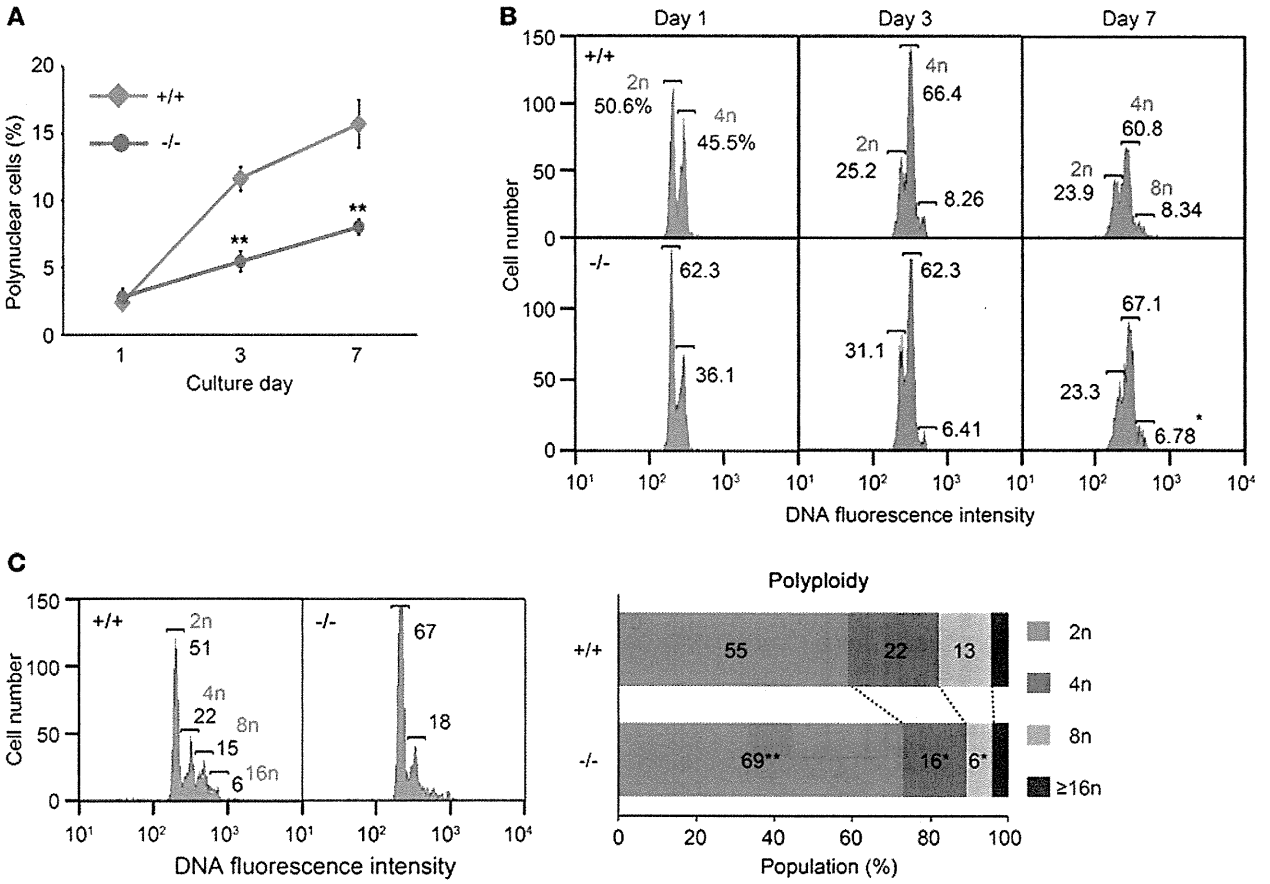

Figure 3

Attenuated polyploidy in *Dedd*$^{-/-}$ decidual cells. (**A**) In vitro decidualizing uterine stromal cells were stained with Hoechst to identify nuclei after different times in culture, and the number of polynuclear cells among 600 cells was counted microscopically. Analysis was performed by 3 independent researchers. (**B** and **C**) Quantification of DNA in in vitro decidualizing uterine stromal cells (**B**) or ex vivo stromal cells isolated from 4.5-dpc implantation sites (**C**). Cells were stained with Hoechst and analyzed by flow cytometry. Three independent experiments were performed, and a representative set of profiles is presented. In **C**, the average sizes for 2n, 4n, 8n, and ≥16n populations are also presented (right panel). $^{**}P < 0.01$.

antiapoptotic effect, in addition to regulation of the cell cycle (29–31). It is also noteworthy that no reproductive defects have been reported in mice deficient in Akt-1, -2, or -3, with the exception of two reports that *Akt1*$^{-/-}$ mice harbor a partial defect in follicular development within the ovary (32, 33). Thus, each Akt isoform may be functionally redundant in supporting fertility, given that *Dedd*$^{-/-}$ mice in which levels of all isoforms of Akt are decreased show a dramatic uterine defect (11). Our finding that the back-expression of Akt-1 efficiently recovered polyploidy in *Dedd*$^{-/-}$ stromal cells may support this idea. Unfortunately, mice doubly or triply deficient for multiple types of Akt die before they reach reproductive age (34). Future creation and analysis of conditional knockout mice in which various types of Akt are specifically deficient in the uterus will help to elucidate the involvement of Akt in fertility.

Perspectives. Our present findings identifying DEDD as an indispensable element in support of early pregnancy might shed light on the pathogenesis of infertility of unknown cause. Indeed, *DEDD* expression in uterine stromal cells increases along with decidualization both in mice and humans. In women experiencing implantation failure, one-third of the failures have been attributed to the embryo itself (35). Although the remaining two-thirds of failures appear to be the result of an inadequate uterine environment, the precise defect is often unknown. Thus, it may be worth addressing whether DEDD dysfunction is present in infertile women, either genetically or functionally, in uterine stromal cells. This may contribute to the development of new therapeutic strategies for infertility, though association of DEDD function with polyploidization as well as Akt and cyclin D3 in humans certainly needs to be further assessed.

Methods

Mice and human specimens. *Dedd*$^{-/-}$ mice had been cross-bred to C57BL/6 for 17 generations before being used for experiments. Female mice of 2–6 months of age were used. The day of the vaginal plug was considered as 0.5 dpc. Pseudopregnant mice were produced by mating female mice with vasectomized male mice of the CD-1 strain. All mice were maintained under specific pathogen-free conditions. All animals used in the experiments were cared for in accordance with institutional guidelines. Human endometrial tissue was obtained from women with benign diseases. The experimental procedures were approved by the institutional review board of the University of Tokyo, and all women provided written informed consent for the use of their endometrial tissue.

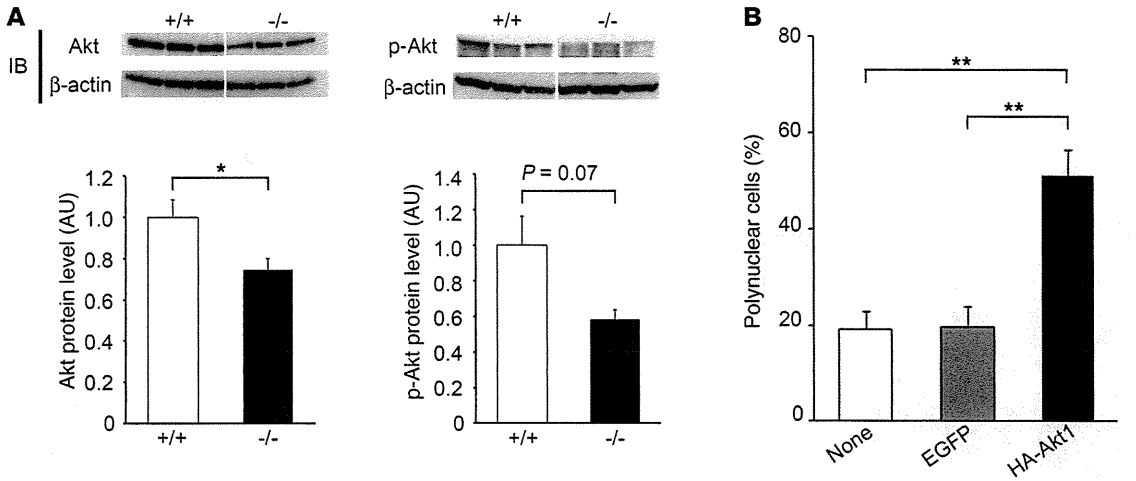

Figure 4

Involvement of Akt level in defective polyploidy in *Dedd*$^{-/-}$ decidual cells. (**A**) Immunoblotting of *Dedd*$^{+/+}$ and *Dedd*$^{-/-}$ uteri at 5.5 dpc for total Akt (left) and phosphorylated Akt (at Thr308, right). Three mice were analyzed. Quantification was performed with NIH Image J software. Values are presented as protein levels relative to those from *Dedd*$^{+/+}$ uteri. Error bars indicate SEM. (**B**) In vitro decidualizing *Dedd*$^{-/-}$ stromal cells were transfected with expression vector for HA-Akt1 or control EGFP at day 2. At day 5, cells were stained for HA and Hoechst; thereafter, the proportion of polynuclear cells among more than 100 HA-positive cells was evaluated microscopically. Average results from 4 independent sets of experiment are presented. Error bars indicate SEM. $^{*}P < 0.05$, $^{**}P < 0.01$.

Reagents and antibodies. Antibodies and reagents used were as follows. Primary antibodies were: ant–COX-2 (polyclonal, Cell Signaling Technology); anti-TIMP3 (W-18, Santa Cruz Biotechnology Inc.); anti-Akt (pan) (11E7, Cell Signaling Technology); anti-Ki67 (SP6, Thermo Scientific); anti-phospho-Akt (Thr308) (244F9, Cell Signaling Technology); anti-cyclin D3 (C-16, Santa Cruz Biotechnology Inc.) for immunohistochemistry; anti-cyclin D3 (DCS-22, Thermo Scientific) for immunoblotting and immunoprecipitation; anti-Cdk4 (DCS-35, Thermo Scientific); anti-Cdk6 (DCS-83, Thermo scientific); anti-β-actin (ACTN05 [C4], Abcam); anti-HA high-affinity antibody (3F10, Roche); and anti-FLAG antibody (M2, Sigma-Aldrich). Secondary antibodies and related reagents were: Alexa Fluor 488–conjugated anti-rabbit IgG antibody (Invitrogen); Alexa Fluor 546–conjugated anti-goat IgG antibody (Invitrogen); Hoechst 33258 and Hoechst 33324 (Invitrogen); Protein Block Serum-Free (Dako Cytomation); normal goat serum (Wako); Mayer's hematoxylin (Muto Pure Chemicals Co. Ltd.); eosin Y solution (Sigma-Aldrich); HRP-conjugated anti-mouse IgG (Pierce); and HRP-conjugated anti-rabbit IgG (Pierce).

Analysis of ovulation and fertilization. Briefly, superovulation was induced by intraperitoneal injection of pregnant mare serum gonadotropin (PMSG) (at -2.5 dpc; 5 IU/mouse) and human chorionic gonadotropin (hCG) (at -0.5 dpc; 5 IU/mouse). Oviducts from mated females were flushed with M2 medium at 0.5 dpc. Under a microscope, numbers of eggs were determined, and fertilization efficiency was evaluated by morphology of the eggs (i.e., having 2 nuclei or a fused large nucleus).

Histologic and immunohistochemical analysis. Uterine specimens were fixed by infusion of 4% PFA. For immunohistochemistry, deparaffinized sections were boiled in 10 mM sodium citrate buffer, pH 6.0, by microwave for 10 minutes. After blocking, sections were incubated with primary antibodies at 4°C for 16 hours, followed by secondary antibodies at room temperature for 1 hour. Samples were counterstained with Hoechst 33258. The areas of TIMP3-positive region and edematous region were measured by ImageJ software (NIH). Similarly, the embryonic area was measured. The size of each embryo was calculated as the sum of the embryonic area multiplied by its thickness (10 μm/section).

In situ hybridization. A 433-bp DNA fragment corresponding to the nucleotide positions 81–513 of mouse *Dedd* was subcloned into pGEMT-Easy vector (Promega) and was used for generation of sense or antisense RNA probes. A 431-bp DNA fragment corresponding to the nucleotide positions 1082–1512 of mouse *cyclin D3* and a 694-bp DNA fragment corresponding to the nucleotide positions 1851–2544 of mouse *Akt1* were similarly prepared. Paraffin-embedded uterine sections (6 μm) were hybridized with digoxigenin-labeled RNA probes at 60°C for 16 hours. The bound label was detected using NBT-BCIP, an alkaline phosphate color substrate. The sections were counterstained with Kernechtrot (Muto Pure Chemicals Co. Ltd.).

Primary culture of uterine stromal cells. The isolation and culture of mouse uterine stromal cells were performed as previously described (36). Briefly, uterine horns on day 3.5 of pseudopregnancy were cut and washed in HBSS (Invitrogen) without Ca^{2+}/Mg^{2+} and phenol red but containing 100 U/ml penicillin and 100 μg/ml streptomycin (Pen Strep; Invitrogen) and 2.5 μg/ml amphotericin B (Sigma-Aldrich). Tissues were digested in HBSS containing 6 mg/ml dispase (Invitrogen) and 25 mg/ml pancreatin (Sigma-Aldrich) and subsequently treated with 0.5 mg/ml collagenase (Sigma-Aldrich). The digested cells were passed through a 70-μm nylon filter to eliminate clumps of epithelial cells and were plated at 5×10^5 cells per 25 cm^2. For in vitro decidualization, the adherent cells were cultured in phenol red–free DMEM and Ham's F-12 nutrient mixture (DMEM/F-12, 1:1) (Invitrogen) with 1% charcoal-stripped FBS (Invitrogen) and antibiotics, 17β-estradiol (E2, 10 nM) (Sigma-Aldrich), P4 (1 μM) (Sigma-Aldrich), and HB-EGF (30 ng/ml) (Sigma-Aldrich). The induction of differentiation was continued for 7 days without changing medium. Isolation and differentiation of human endometrial stromal cells were performed as described previously (37). Cells were treated with phenol red–free DMEM/F-12 containing 5% charcoal-stripped FBS, antibiotics, E2 (10 ng/ml), and P4 (100 ng/ml) for 12 days. Media were replenished every 3 days.

Analysis of cell cycle and polyploidization. Cell cycle was analyzed using the Click-iT EdU kit (Invitrogen). Cultured uterine stromal cells were harvested at days 1, 3, and 7 after 10 μM EdU incorporation for 2 hours each. Trypsinized cells were fixed with 4% PFA and permeabilized with saponin. Incorporated EdU

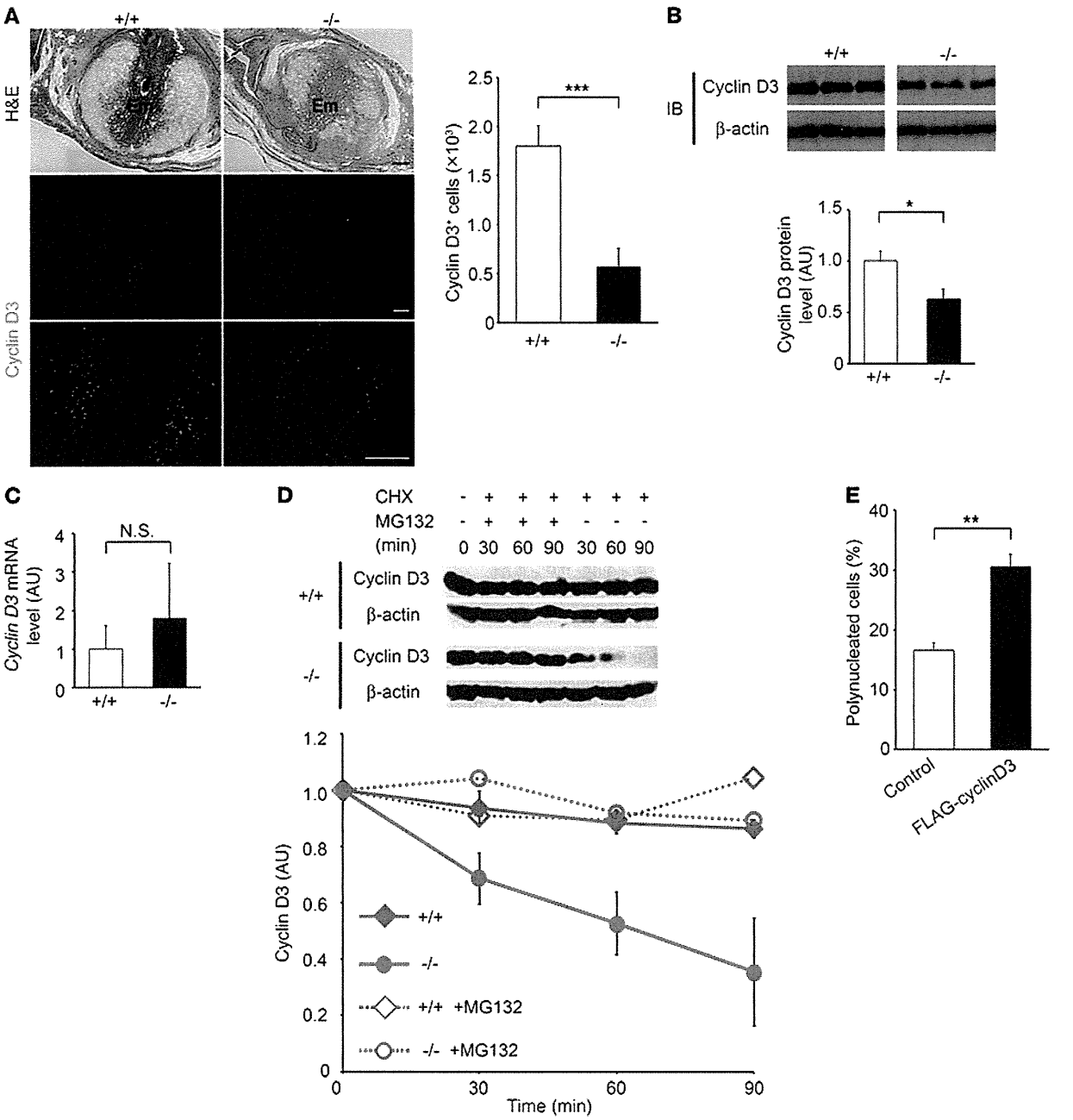

Figure 5

Decreased stability of cyclin D3 protein in *Dedd*$^{-/-}$ decidual cells. (**A**) At 5.5 dpc, implantation sites in *Dedd*$^{+/+}$ and *Dedd*$^{-/-}$ uteri were immunostained for cyclin D3. Bottom panels show higher magnifications of the dotted area in the middle panels. Scale bars: 200 μm. Graph on the right: Cyclin D3–positive cells within an implantation site were counted and compared in at least 4 different sections, and the means are presented. Error bars indicate SEM. (**B**) Immunoblotting of *Dedd*$^{+/+}$ and *Dedd*$^{-/-}$ uteri at 5.5 dpc for cyclin D3 and quantification of results. Three mice were analyzed. Error bars indicate SEM. (**C**) mRNA level for *cyclin D3* in 5.5-dpc implantation sites. No significant decrease in mRNA level was detected in *Dedd*$^{-/-}$ cells and tissues ($n = 3$ for each). (**D**) Protein degradation assay for cyclin D3. Uterine stromal cells at day 3 of in vitro decidualization were treated with cycloheximide (CHX; 50 μM) for the indicated periods in the presence or absence of proteasome inhibitor MG132 (10 μM). At each time point, cells were harvested, and the lysate was analyzed for cyclin D3 by immunoblotting. The amount of cyclin D3 protein at each time point was normalized to that of β-actin and is presented as relative level to that at pretreatment (0 minutes) in *Dedd*$^{+/+}$ or *Dedd*$^{-/-}$ cells. Three independent experiments were performed, and representative blots are presented. Error bars indicate SEM. (**E**) In vitro decidualizing *Dedd*$^{-/-}$ stromal cells were transfected with expression vector for FLAG–cyclin D3 at day 2. At day 5, cells were stained for FLAG and Hoechst; thereafter, the proportion of polynuclear cells among more than 100 FLAG-positive cells was evaluated microscopically. Average results from 4 independent sets of experiment are presented. Error bar indicate SEM. $^{*}P < 0.05$, $^{**}P < 0.01$, $^{***}P < 0.001$.

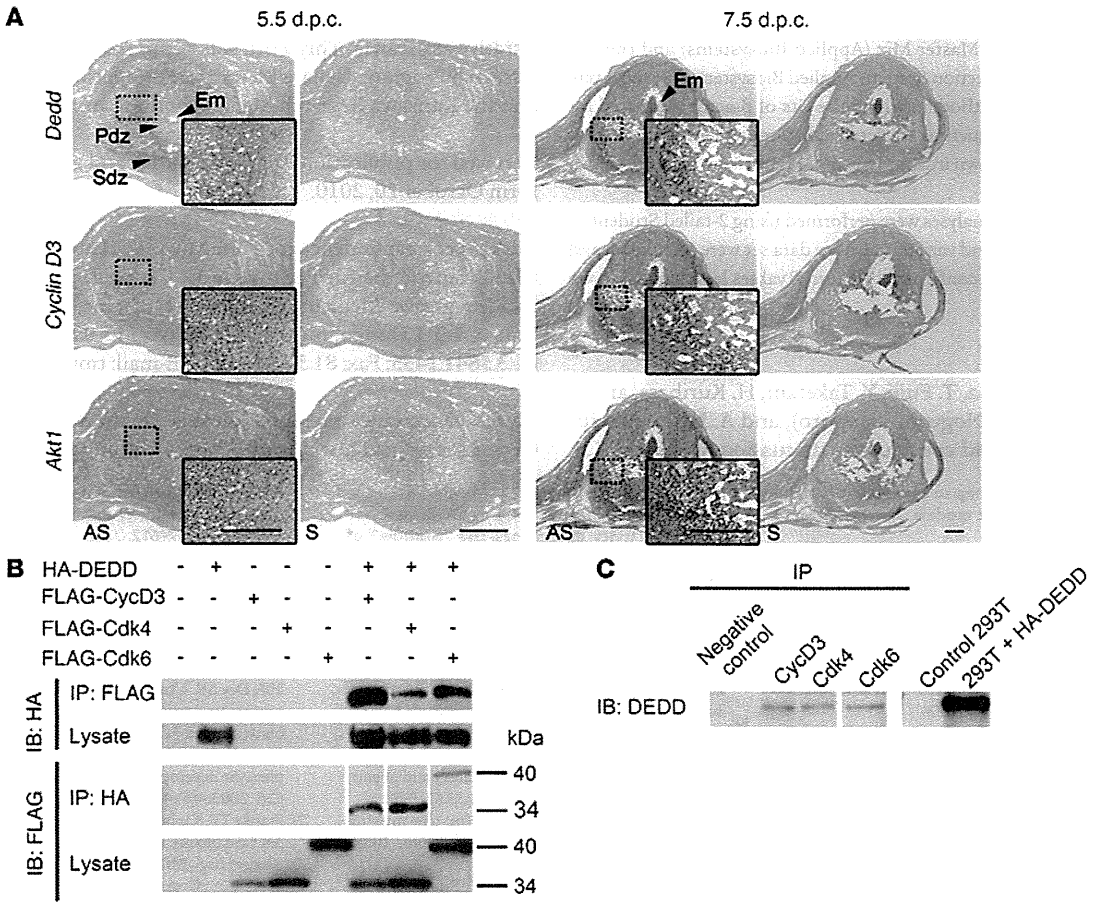

Figure 6

The association of DEDD with cyclin D3. (**A**) In situ mRNA analysis for *Dedd*, *cyclin D3*, and *Akt1* in 5.5- and 7.5- dpc wild-type mouse uteri. Microphotographs at a higher magnification are also presented. AS, antisense probe; S, sense control probe; Pdz, primary decidual zone; Sdz, secondary decidual zone. Scale bars: 500 μm. (**B**) Binding study. HA-tagged DEDD and FLAG-tagged cyclin D3, Cdk4, or Cdk6 were expressed in HEK293T cells, and association of HA-DEDD and each FLAG-tagged protein was evaluated by a coimmunoprecipitation assay with anti-HA or anti-FLAG antibody. (**C**) Coprecipitation of endogenous DEDD with cyclin D3, Cdk4, or Cdk6 from lysates of 5.5-dpc uterine implantation sites. Precipitates were immunoblotted with an anti-DEDD antibody. HEK293T cells with or without transfection of HA-tagged DEDD were used as controls.

was detected by an alkylation reagent conjugated with Alexa Fluor 488. DNA content was quantitatively detected by subsequent staining with Hoechst 33342. At least 10,000 cells for each sample were analyzed by flow cytometry. For evaluation of polyploidy, cells were cultured in a 4-well chamber and stained with Hoechst after fixation with 4% PFA. Multinucleated cells were calculated under a fluorescence microscope and counted by 3 independent researchers in a blinded fashion from more than 600 total cells each.

Flow cytometry (analysis of cell DNA contents). In vitro decidualizing cells were stained with Hoechst 33342 and analyzed for DNA content by an LSR II flow cytometer (BD). At least 10,000 cells were analyzed for each. For ex vivo cells, 4.5-dpc uterine implantation sites were digested by a collagenase treatment, and purified single cells were stained with Hoechst 33342. The large stromal cell population was gated, and at least 1,000 cells were analyzed for DNA content.

Akt and cyclin D3 overexpression in decidual cells. Uterine stromal cells at day 2 of culture in the presence of E2, P4, and HB-EGF were transfected with a pCruz-HA-Akt1, pFLAG-cyclinD3, or a mock expression vector by using Lipofectamine 2000 (Invitrogen). At day 5, cells were fixed with 4% PFA and permeabilized with 0.25% Triton X-100. The transfected cells were detected by anti-HA high-affinity antibody or anti-FLAG antibody conjugated with Cy3. Multinucleated cells were counted under a fluorescence microscope after Hoechst staining.

Protein degradation assay. Day 3 in vitro decidualizing stromal cells were treated with 50 μM cycloheximide (Sigma-Aldrich) in the presence or absence of 10 μM MG132 (Sigma-Aldrich) and were harvested at the indicated time points. Cells were lysed in a lysis buffer (1% NP-40, 150 mM NaCl, 50 mM Tris-HCl pH 7.4, 1 mM sodium orthovanadate, 1 mM sodium fluoride, and Complete Mini [Roche]) and used for immunoblotting.

Coimmunoprecipitation assay. HEK293T cells were transfected with pCAG-DEDD-HA, pFLAG-cyclin D3, pFLAG-Cdk4, or pFLAG-Cdk6 by electroporation. Cells were lysed and incubated with anti-HA or anti-FLAG beads for 16 hours at 4°C. Precipitates were analyzed for the presence of coprecipitated molecule by immunoblotting using anti-FLAG or anti-HA antibody. For the binding of endogenous DEDD with cyclin D3, Cdk4, or Cdk6, 5.5-dpc uterine implantation sites were homogenized in lysis buffer and incubated with anti–cyclin D3, anti-Cdk4, or anti-Cdk6 antibody bound to protein G beads. Precipitates were immunoblotted with an anti-DEDD polyclonal antibody prepared in-house (8).

Quantitative and semiquantitative RT-PCR. QPCR was performed using Power SYBR Green PCR Master Mix (Applied Biosystems) and the ABI Prism 7000 Sequence Detection System (Applied Biosystems). Results were analyzed by the ΔΔCt method, in which the Cts of β-actin were used for normalization. Primer sequences are detailed in Supplemental Table 1. For semiquantitative PCR shown in Supplemental Figure 3, primers are shown in Supplemental Table 2.

Statistics. All statistical analyses were performed using 2-tailed Student's *t* test. Standard deviation and variance of every data set were calculated, and the homoscedasticity was confirmed by *F* test. *P* values less than 0.05 were considered significant.

Acknowledgments

We thank to A. Kodama, T. Fujii, Y. Taketani, H. Kurihara, and Y. Kurihara (Tokyo), M. Noguchi (Sapporo), and A. Nishijima, for technical assistance and constructive discussion; Genostaff Co. Ltd. for in situ mRNA hybridization; and M. Miyamoto for administrative assistance. This work was supported by the Global COE Research Program, Uehara Memorial Foundation (to T. Miyazaki), and the Kanzawa Research Medical Foundation (to S. Arai).

Received for publication August 12, 2010, and accepted in revised form October 20, 2010.

Address correspondence to: Toru Miyazaki, Laboratory of Molecular Biomedicine for Pathogenesis, Center for Disease Biology and Integrative Medicine, Faculty of Medicine, The University of Tokyo, 7-3-1 Hongo, Bunkyo-ku, Tokyo 113-0033, Japan. Phone: 81.3.5841.1435; Fax: 81.3.5841.1438; E-mail: tm@m.u-tokyo.ac.jp.

Miwako Kitazume's present address is: Division of Developmental Genetics, National Institute of Genetics, Mishima, Shizuoka, Japan.

1. Wang H, Dey SK. Roadmap to embryo implantation: clues from mouse models. *Nat Rev Genet.* 2006;7(3):185–199.
2. Dey SK, et al. Molecular cues to implantation. *Endocr Rev.* 2004;25(3):341–373.
3. Das SK. Cell cycle regulatory control for uterine stromal cell decidualization in implantation. *Reproduction.* 2009;137(6):889–899.
4. Satokata I, Benson G, Maas R. Sexually dimorphic sterility phenotypes in Hoxa10-deficient mice. *Nature.* 1995;374(6521):460–463.
5. Lim H, Ma L, Ma WG, Maas RL, Dey SK. Hoxa-10 regulates uterine stromal cell responsiveness to progesterone during implantation and decidualization in the mouse. *Mol Endocrinol.* 1999;13(6):1005–1017.
6. Robb L, Li R, Hartley L, Nandurkar HH, Koentgen F, Begley CG. Infertility in female mice lacking the receptor for interleukin 11 is due to a defective uterine response to implantation. *Nat Med.* 1998;4(3):303–308.
7. Tan J, Raja S, Davis MK, Tawfik O, Dey SK, Das SK. Evidence for coordinated interaction of cyclin D3 with p21 and cdk6 in directing the development of uterine stromal cell decidualization and polyploidy during implantation. *Mech Dev.* 2002; 111(1-2):99–113.
8. Arai S, et al. Death-effector domain-containing protein DEDD is an inhibitor of mitotic Cdk1/cyclin B1. *Proc Natl Acad Sci U S A.* 2007;104(7):2289–2294.
9. Miyazaki T, Arai S. Two distinct controls of mitotic cdk1/cyclin B1 activity requisite for cell growth prior to cell division. *Cell Cycle.* 2007;6(12):1419–1425.
10. Kurabe N, et al. The death effector domain-containing DEDD supports S6K1 activity via preventing Cdk1-dependent inhibitory phosphorylation. *J Biol Chem.* 2009;284(8):5050–5055.
11. Kurabe N, et al. The death effector domain-containing DEDD forms a complex with Akt and Hsp90, and supports their stability. *Biochem Biophys Res Commun.* 2010;391(4):1708–1713.
12. Pende M, et al. Hypoinsulinaemia, glucose intolerance and diminished beta-cell size in S6K1-deficient mice. *Nature.* 2000;408(6815):994–997.
13. Paria BC, Huet-Hudson YM, Dey SK. Blastocyst's state of activity determines the "window" of implantation in the mouse receptive uterus. *Proc Natl Acad Sci U S A.* 1993;90(21):10159–10162.
14. Lim H, et al. Multiple female reproductive failures in cyclooxygenase 2-deficient mice. *Cell.* 1997;91(2):197–208.
15. Bany BM, Schultz GA. Tissue inhibitor of matrix metalloproteinase-3 expression in the mouse uterus during implantation and artificially induced decidualization. *Mol Reprod Dev.* 2001;59(2):159–167.
16. Hassan MQ, et al. HOXA10 controls osteoblastogenesis by directly activating bone regulatory and phenotypic genes. *Mol Cell Biol.* 2007;27(9):3337–3352.
17. Lee KY, et al. Bmp2 is critical for the murine uterine decidual response. *Mol Cell Biol.* 2007; 27(15):5468–5478.
18. Diehl JA, Cheng M, Roussel MF, Sherr CJ. Glycogen synthase kinase-3beta regulates cyclin D1 proteolysis and subcellular localization. *Genes Dev.* 1998;12(22):3499–3511.
19. Das SK. Regional development of uterine decidualization: molecular signaling by Hoxa-10. *Mol Reprod Dev.* 2010;77(5):387–396.
20. Das SK, Lim H, Paria BC, Dey SK. Cyclin D3 in the mouse uterus is associated with the decidualization process during early pregnancy. *J Mol Endocrinol.* 1999;22(1):91–101.
21. García-Morales P, Hernando E, Carrasco-García E, Menéndez-Gutierrez MP, Saceda M, Martínez-Lacaci I. Cyclin D3 is down-regulated by rapamycin in HER-2-overexpressing breast cancer cells. *Mol Cancer Ther.* 2006;5(9):2172–2181.
22. Sachs L, Shelesnyak MC. The development and suppression of polyploidy in the developing and suppressed deciduoma in the rat. *J Endocrinol.* 1955; 12(2):146–151.
23. Ansell JD, Barlow PW, McLaren A. Binucleate and polyploid cells in the decidua of the mouse. *J Embryol Exp Morphol.* 1974;31(1):223–227.
24. Moulton BC. Effect of progesterone on DNA, RNA and protein synthesis of deciduoma cell fractions separated by velocity sedimentation. *Biol Reprod.* 1979;21(3):667–672.
25. Edgar BA, Orr-Weaver TL. Endoreplication cell cycles: more for less. *Cell.* 2001;105(3):297–306.
26. Yang ZZ, et al. Protein kinase B alpha/Akt1 regulates placental development and fetal growth. *J Biol Chem.* 2003;278(34):32124–32131.
27. Hirota Y, Daikoku T, Tranguch S, Xie H, Bradshaw HB, Dey SK. Uterine-specific p53 deficiency confers premature uterine senescence and promotes preterm birth in mice. *J Clin Invest.* 2010;120(3):803–815.
28. Sicinska E, et al. Requirement for cyclin D3 in lymphocyte development and T cell leukemias. *Cancer Cell.* 2003;4(6):451–461.
29. Franke TF, Kaplan DR, Cantley LC. PI3K: downstream AKTion blocks apoptosis. *Cell.* 1997;88(4):435–437.
30. Burgering BM, Coffer PJ. Protein kinase B (c-Akt) in phosphatidylinositol-3-OH kinase signal transduction. *Nature.* 1995;376(6541):599–602.
31. Franke TF. Intracellular signaling by Akt: bound to be specific. *Sci Signal.* 2008;1(24):pe29.
32. Brown C, et al. Subfertility caused by altered follicular development and oocyte growth in female mice lacking PKBalpha/Akt. *Biol Reprod.* 2010;82(2):246–256.
33. Easton RM, et al. Role for Akt3/protein kinase Bgamma in attainment of normal brain size. *Mol Cell Biol.* 2005;25(5):1869–1878.
34. Peng XD, et al. Dwarfism, impaired skin development, skeletal muscle atrophy, delayed bone development, and impeded adipogenesis in mice lacking Akt1 and Akt2. *Genes Dev.* 2003;17(11):1352–1365.
35. Simón C, Moreno C, Remohí J, Pellicer A. Cytokines and embryo implantation. *J Reprod Immunol.* 1998;39(1-2):117–131.
36. Tan Y, et al. HB-EGF directs stromal cell polyploidy and decidualization via cyclin D3 during implantation. *Dev Biol.* 2004;265(1):181–195.
37. Kodama A, et al. Progesterone decreases bone morphogenetic protein (BMP) 7 expression and BMP7 inhibits decidualization and proliferation in endometrial stromal cells. *Human Reprod.* 2010;25(3):751–756.